DELFT UNIVERSITY OF TECHNOLOGY
Department of Electrical Engineering
Telecommunications and Traffic Control Systems Group

# Wideband channel measurements at 60 GHz in different environments

Author : A.R. Mank

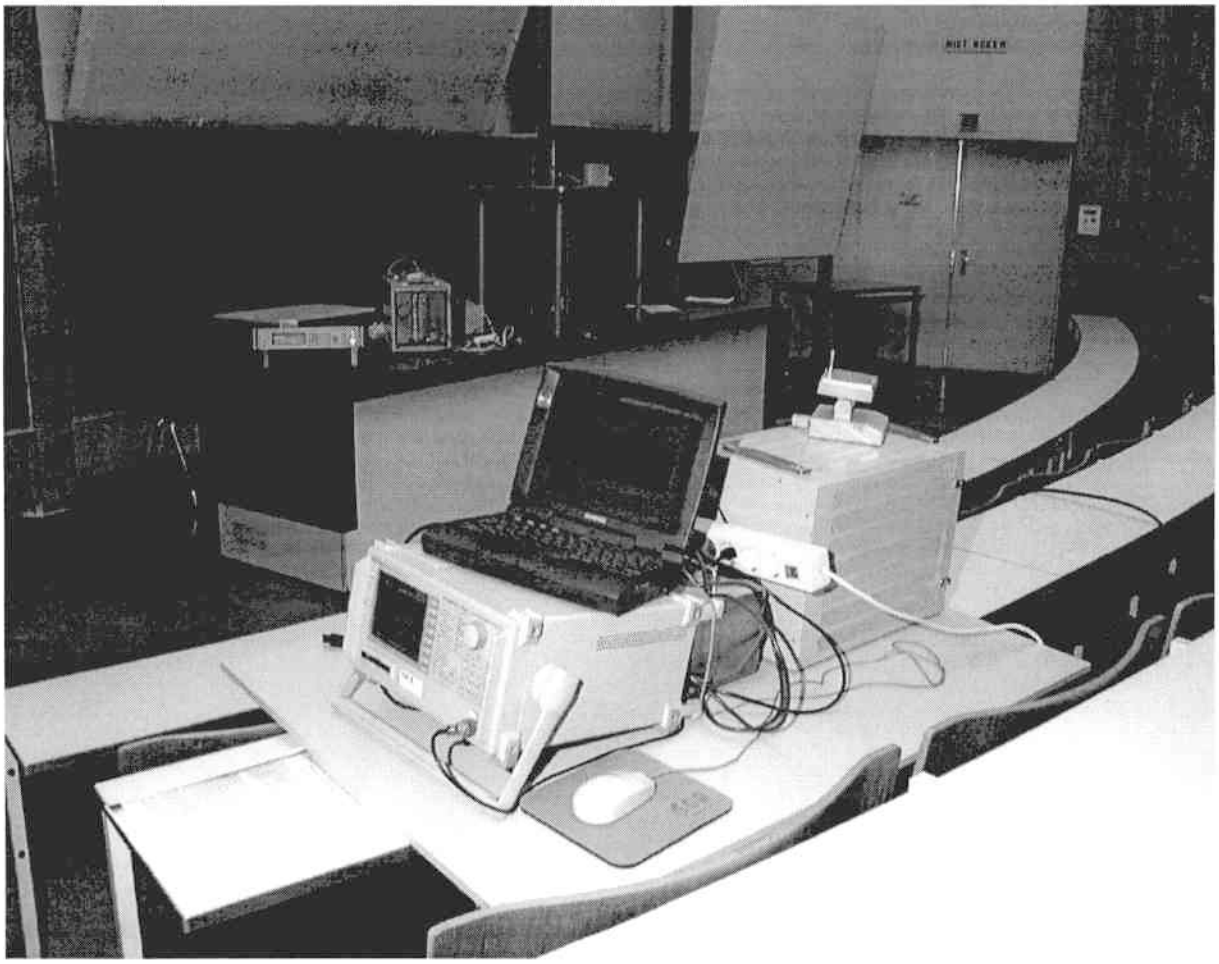

| | |
|---|---|
| Professor : | Prof. R. Prasad |
| Mentors : | Ir. D. Matic, Ir. K. Witrisal |

| | |
|---|---|
| Type : | Thesis Report |
| Period : | October 1997 – July 1998 |
| Date : | 24 August 1998 |
| Number of pages : | 53 |
| Graduation number : | A-816 |

## Preface

This report is the result of my thesis work performed at the Department of Telecommunications and Traffic Control Systems, Faculty of Electrical Engineering, Delft University of Technology. It was part of a project called MMC: Mobile Multimedia Communications (more information available at http://mmc.et.tudelft.nl) and a project called M5: a cooperation with NEC and the Department of Telecommunications and Traffic Control Systems. NEC is responsible for the delivery of the necessarily measurement equipment. Within the MMC project several kinds of problems (in all different OSI-layers) were examined for future MMC systems like: What kind of applications will be a success, how shall the user-interface look like, what kind of compression and protocols will be suitable, how should the transmission be done? Because of the broad range of problems, the project is divided in several groups. This report is about work done within the transmission group.

I would like to thank all the people who contribute to my thesis work, especially:
Ramjee Prasad as my thesis docent,
Dusan Matic as my thesis mentor,
Klaus Witrisal and Gerard Janssen for their help in analyze work,
Herman Stikkel, Han Reymers and the two French guys Vincent Macaux and Guillaume Roughling for their support with measuring,
NEC for the delivery of the measuring equipment and
of course, the other thesis students who were a good company to work with.

Arthur Mank,

17 - 08 -1998, Delft

## Abstract

For future mobile multimedia communication, a Mobile Broadband System is in development, which operates at a frequency of 60 GHz. In order to get a better understanding of 60 GHz propagation effects in different environments with different conditions, several measurements were performed, using a spectrum analyzer and synthesized signal generator for the frequency-domain characterization of the radio channel. In the experiments, a carrier wave (CW) was swept with constant amplitude across the 100 MHz band, centered on 59.9 GHz. The channel frequency response was measured at the receiver side. The results can be used for the design of an OFDM (Orthogonal Frequency Division Multiplex) system.

The measurement environments were a corridor and a big college room in a high-rise office building (indoor) and a parking and a grassfield at the side of that building (outdoor). The spectrum samples were taken in each of the environments. From such samples, parameters that describe the wireless channel can be calculated like the Rice parameter *k,* the path loss coefficients, coherence bandwidth and the delay spread. It was necessary to develop an appropriate measurement analysis, stemming from the fact that the spectrum analyzer gives no information on the phase, only amplitude. Measurement analysis method and results are explained. When more and more dense measurements are performed a more detailed and accurate description of the wireless channel for the different environments is possible.

## Index terms

60 GHz, measurements, wideband, multipath, channel modeling, channel parameters, Rice factor *k*, path loss, coherence bandwidth, delay spread, indoor, outdoor

# List of symbols and abbreviations

Symbols

| | |
|---|---|
| $\alpha$ | path loss factor |
| $\beta_0$ | direct path amplitude |
| $\beta_0^2$ | the power of the direct ray |
| $\beta_m$ | *m*th ray amplitude gain |
| d | distance |
| H(f) | complex impulse response in frequency-domain |
| h(t) | complex impulse response in time-domain |
| I1 | Corridor (Indoor) |
| I2 | Amphitheater (Indoor) |
| $\Pi$ | the power-density of the constant-level part |
| $k$ | Rician factor |
| $\bar{k}$ | Average value of Rice factor $k$ |
| O1 | Grassfield (Outdoor) |
| O2 | Parking (Outdoor) |
| $\sigma_k$ | standard deviation of Rice factor $k$ |
| $\sigma_{P(f)}^2$ | variance of $P(f)$ |
| $\theta_m$ | *m*th ray phase |
| $p(0)$ | the power of the direct ray |
| $P_t$ | transmitter power |
| $P_r$ | received power |
| $r$ | correlation |
| $R(\Delta f)$ | frequency correlation function |
| $\tau_1$ | the turning point |
| $\tau_m$ | *m*th ray time delay. |

## Abbreviations

| | |
|---|---|
| 8PSK | 8 Phase Shift Keying |
| BW | Bandwidth |
| cdf | cumulative distribution function |
| CW | Carrier Wave |
| EE | Electrical Engineering |
| GPIB | General Purpose Information Bus |
| GSM | Global System for Mobile communications |
| ISI | Inter Symbol Interference |
| IF | Intermediate Frequency |
| lcr | level crossing rate |
| LOS | Line-of-Sight |
| M5 | Project of NEC and TVS |
| MBS | Mobile Broadband System |
| MMC | Mobile Multimedia Communication |
| pdf | probability distribution function |
| OFDM | Orthogonal Frequency Digital Modulation |
| OSI | Open Systems Interconnection |
| R | Receiver |
| RF | Radio Frequency |
| rms | root mean square |
| T | Transmitter |
| UMTS | Universal Mobile Telecommunications System |

# Table of Contents

## Introduction

In today's telecommunications with its mobile communication GSM network and the Internet the need for more mobile and more multimedia services are visible. Mobility means more flexibility (usable at any place) and multimedia is more appealing than just speech and is also a result of the integration of telecommunication and information technology. The consequence is that the services/ applications run over the (mobile) telecommunication network demand an increasing amount of bandwidth.

The GSM network is mainly meant for speech communication (bitrates of 9.6 Kb/s), but a third generation (GSM is the second generation) is already in development: Universal Mobile Telecommunication Systems (UMTS). With UMTS bitrates of 2 Mb/s are feasible. UMTS should be operational in about 5 years. For even higher bit-rates, a fourth generation network for mobile communication is also in development: Mobile Broadband Systems (MBS) [1,2]. With this MBS applications which require bitrates of 155 Mb/s should be possible. MBS is planned to be operational in about 10 until 15 years from now.

With these mobile communications systems with high bitrates and it's broad range of services we're going more and more towards a "Global Village": to offer any communication-service from every person to every random other person at any place without delay via any communication medium using personal communication numbers.

A large bandwidth is needed for the mobile multimedia applications, which ask for bitrates of 2-150 Mb/s. Because of the high bit rate demands, higher frequencies are needed. A suitable frequency for MBS is 60 GHz.

Why 60 GHz?

There are four main advantages [1,2]:
1. There is a great range of bandwidth available and it supports broadband service access
2. Almost none co-channel interference (because of high oxygen-absorption, 15 dB/km)
3. This frequency region is not in use by any other communication system
4. Small dimensions of the antennas (range of cm, because of wavelength of 5 mm)

Although there are also some drawbacks (small range of cell (50-100 m), only low power can be used because of health hazards, multipath effects, radio-path may not be too obstructed by obstacles) 60 GHz is considered to be a good candidate for MBS. Because it is quite a new technology, not much research is done at 60 GHz.

In order to develop a good mobile communication system, a good understanding of the radio propagation is crucial.

The transmission over the wireless communication channel (the physical layer of the OSI-model), which is in a hostile environment is subject to effects as multipath, obstruction and shadowing. Multipath effects arise in situations where there are several paths over which a radio-signal can travel and those different rays interfere with each other and cause destruction of the signal. Obstruction and shadowing arise where there is no Line-of-Sight signal for the transmission path. Solutions to overcome these situations are space diversity, antenna diversity, equalization, error correction and other.

In this report, transmission aspects at 60 GHz have been examined. Through channel measurements over a bandwidth of 100 MHz an insight into the transmission aspects is made.

The main objective of the indoor radio wave propagation measurements is to determine the radio-coverage and data-rate limitations. [3,4]. The radio-coverage is related to the distance -power relationship in the area, and data rate is limited by the frequency selective fading multipath characteristics of the channel.

The transmission channel can be described by parameters that are extracted out of these measurements. Because every environment has it's own characteristics, each environment has different parameter values. But instead of using measurements to determine transmission effects, these parameters can be a more efficient way to describe the transmission model for each environment. It is not as time-consuming as measuring every time and still it has the ability to describe the channel accurately enough.

In Chapter 1, the mobile multipath channel will be discussed; the actual measurements are described in Chapter 2 and in Chapter 3 they will be analyzed. Finally, in Chapter 4 the conclusions and recommendations that can be made will be given.

# 1. The mobile multipath channel

For a carrier frequency of several GHz, the wavelength is in the order of mm's, in fact 5 mm for 60 GHz. This short wavelength has a strong effect on the wireless channel's propagation effects.

## *1.1 Propagation aspects*

What propagation aspects play a role in the wireless communication channel [5,6]?

Basically, propagation effects can be divided into three categories:

1. Path loss
2. Large scale multipath fading
3. Small scale multipath fading

1. Path loss

This is the first approximation of the channel. Assumed that no other effects play a role than a decreasing power with increasing distance, the received power can be described by:

$$P_r(d) = Ad^{-\alpha} \tag{1}$$

in which $P_t$ is the fixed transmitter power, $P_r$ is the received power, d is the distance, A is a constant set by transmitted power and measurement system gain and $\alpha$ is the path loss factor, depending on the transmission medium (assuming an isotropic antenna pattern). For free space, it is 2, but it can range from 1 - 6.

In a wireless mobile communication system, a signal can travel from transmitter to receiver over multiple reflective paths; this phenomenon is referred to as *multipath* propagation. The effect can cause fluctuations in the received signal's amplitude, phase and angle of arrival, giving rise to the terminology *multipath fading*. This multipath fading can be split into two categories: Large scale and small scale multipath fading.

2. Large scale multipath fading

Large scale fading represents the average signal power attenuation or path loss due to motion over large areas (multiple wavelengths). This phenomenon is affected by prominent environment contours, like building material. The receiver is often represented as being "shadowed" by such prominence. This large-scale fading often causes a variation of the received power around the path loss figure, which can be described by a log-normal probability distribution function.

3. Small scale multipath fading

Small-scale fading refers to the dramatic changes in signal amplitudes and phase that can be experienced as a result of changes (as small as a wavelength) in the spatial separation between a receiver and transmitter. The probability distribution function of the received power because of this small-scale fading can be described by a Rayleigh or Rician distribution [4, Ch. 3 and 4]; depending on the strength of the Line-of-Sight component (LOS), which is the direct ray component between the receiver and the transmitter antenna. If there is a strong LOS-component, the Rician distribution is applicable, if the LOS-component is comparable with the interfering components, the Rayleigh distribution should be used. The Rician distribution is defined by the Rician factor *k*, and if $k << 1$, the Rayleigh distribution is applicable.

Besides the distance, also time and frequency (although these are implicit in the multipath effects hidden) play a role in the propagation of the electromagnetic waves. Especially in case of a mobile wireless communication channel, the channel is also time variant. That means that either the receiver or transmitter antenna has moved or the surrounding environment changes in time.

For a wideband signal, the fading is not frequency-independent. Wideband means that bandwidth of the signal is bigger than the coherence bandwidth. Within coherence bandwidth, we have flat fading. If the signal has a bigger bandwidth than that, "drops" of the signal level can be observed in some parts of the spectrum. That is caused because a number of reflected signals approach receiver antenna and sum together. This can be destructive for some frequencies. That is called frequency selective fading.

### *1.2 Measurement methods*

There are several ways of measuring the propagation channel, but they are all based on time, frequency-domain or correlation measurements. Most 60 GHz measurements were done in the time-domain. Time and frequency are completely dual (through the Fourier Transform). These measurement techniques can be classified as *direct pulse measurements*, *spread spectrum sliding correlation measurements*, and *swept frequency measurements*[4, Ch. 3 and 4]. Non-coherent measurements yield only information about the received power and amplitude, coherent measurements also yield phase information.

Direct pulse measurements [7,8]:
This simple channel sounding technique allows engineers to determine the power delay profile of any channel. The system transmits a repetitive pulse and uses a receiver with a wide bandpass filter. The signal is then amplified, detected with an envelope detector, displayed and stored on a high-speed oscilloscope. This gives an immediate measurement of the square of the channel impulse response convolved with the probing pulse. If the oscilloscope is set on averaging mode, then this system can provide a local average power delay profile. Another attractive aspect of this system is the lack of complexity, since off-the-shelf equipment can be used. The minimum resolvable delay between multipath components is equal to the probing pulse width.
The main problem with this system is that it is subject to interference and noise, due to the wide bandpass filter, required for multipath time resolution. Also, the pulse system relies on the ability to trigger the oscilloscope on the first arriving signal. If the first arriving signal is blocked or fades, severe fading occurs, and it is possible that the system may not trigger properly. Another disadvantage is that the phases of the individual multipath components are not received, due to the use of an envelope detector. However, use of a coherent detector permits measurement of the multipath phase using this technique.

Spread spectrum sliding correlation measurements:
In a spread spectrum channel sounder, a carrier signal is "spread" over a large bandwidth by mixing it with a binary pseudo-noise (PN) sequence having a chip duration $T_c$ and a chip rate $R_c$ equal to $1/T_c$ Hz. The spread spectrum signal is then received, filtered, and despread using a PN sequence generator identical to that used at the transmitter. Although the two PN sequences are identical, the transmitter chip clock is run at slightly faster rate than the receiver chip clock. Mixing the chip sequences in this fashion implements a *sliding correlator*. When the PN code of the faster chip clock catches up with the PN code of the slower chip clock, the two chip sequences will be virtually identically aligned, giving maximal correlation. When the two sequences are not maximally correlated, mixing the incoming spread spectrum signal with the unsynchronized receiver chip sequence will spread this signal into a bandwidth at least as large as the receiver's reference PN sequence. In this way, the narrowband filter that follows the correlator can reject almost all of the incoming signal power. This is how processing gain is realized in a spread spectrum receiver and how it can reject passband interference, unlike the direct pulse sounding system. When the incoming signal is correlated with the receiver sequence, the signal is collapsed back to the original bandwidth (i.e. "despread"), envelope detected, and displayed on an oscilloscope. Since different incoming multipaths will have different time delays, they will maximally correlate with the receiver PN sequence at different times. The energy of these individual paths will pass through the correlator depending on the time delay. Therefore, after envelope detection, the channel impulse response convolved with the pulse shape of a single chip is displayed on the oscilloscope. The time resolution is equal to or greater than $2T_c$.

There are several advantages to the spread spectrum channel sounding system. One of the key spread spectrum modulation characteristics is the ability to reject passband noise, thus improving the coverage range for a given transmitter power. Transmitter and receiver PN sequence synchronization is eliminated by the sliding correlator. Also, required transmitter power can be considerably lower than comparable direct pulse systems due to the inherent "processing gain" of spread spectrum systems.

A disadvantage of the spread spectrum system, as compared to the direct pulse system, is that measurements are not made in real time, but they are compiled as the PN codes slide past one another. Depending on system parameters and measurement objectives, the time required to make power delay profile measurements may be excessive. Another disadvantage of the system describe here is that a non-coherent detector is used, so that phases of individual multipath components can not be measured. Even if coherent detection used, the sweep time of a spread spectrum signal induces delay such that the phases of individual multipath components with different time delays would be measured at substantially different times, during which the channel might change. Another problem is the high chip rate at which the codes are generated which should be much more than the carrier frequency and is not practical for 60 GHz measurements.

Swept frequency measurements [9]:
Because of the dual relationship between time domain and frequency domain techniques, it is possible to measure the channel impulse response in the frequency domain, i.e. with frequency domain channel sounders. A vector network analyzer controls a synthesized frequency sweeper, and an S-parameter test set is used to monitor the frequency response of the channel. The sweeper scans a particular frequency band (centered on the carrier) by stepping through discrete frequencies. The number and spacings of these frequency steps impact the time resolution of the impulse response measurement. For each frequency step, the S-parameter test set transmit a known signal level at port 1 and monitors the received signal level at port 2.

These signal levels allow the analyzer to determine the complex impulse response (i.e. transmissivity) of the channel over the measured frequency range. The transmissivity response is a frequency domain representation of the channel impulse response. This response is then converted to the time domain representation of the channel impulse response. This response is then converted to the time domain using inverse discrete Fourier transform (IDFT) processing, giving a band-limited version of the impulse response.

In theory, this technique works well and indirectly provides amplitude and phase information in the time domain. However, the system requires careful calibration and hardwired synchronization between the transmitter and receiver, making it useful only for very close measurements (e.g. indoor channel sounding). Another limitation with this system is the non-real-time nature of the measurements. For time varying channels, the channel frequency response can change rapidly, giving an erroneous impulse response measurement. To mitigate this effect, fast sweep times are necessary to keep the total swept frequency response measurement interval as short as possible. A faster sweep time can be accomplished by reducing the number of frequency steps, but this sacrifices time resolution and excess delay range in time domain.

### *1.3 Parameters of the mobile multipath channel*

The propagation channel can completely be described by its transfer function H(f) or its h(t), either in the frequency or time-domain. The transfer function model is defined by the amplitudes, phases and delays of each separated propagation ray:

$$h(t)=\sum_{m=0}^{N}\beta_m e^{j\theta_m}\delta(t-\tau_m) \xleftrightarrow{FT} H(f)=\sum_{m=0}^{N}\beta_m e^{j(2\pi f\tau_m+\theta_m)} \tag{2}$$

where $\beta_m$ is the amplitude gain, $\theta_m$ is the phase, $\tau_m$ is the time delay of the *m*th signal reflection.

The path loss can be described by the *path loss parameter* α (1).

For the description of the multipath effects, there are several important parameters. From time-domain measurements a *power delay profile;*

$$P(\tau)=k_1\left|h(\tau)^2\right| \tag{3}$$

where $k_1$ is a constant depending on transmitted power, can be extracted which describes the received power in time when a pulse was transmitted. That way an impression is made about the delays of the propagation rays and the fading the rays undergo while propagating the channel.

This is described by a parameter called the root mean square (rms) *delay spread*;

$$\sigma_\tau=\sqrt{\overline{\tau^2}-(\overline{\tau})^2} \tag{4}$$

where the mean excess delay is

$$\overline{\tau}=\frac{\sum_k P(\tau_k)\tau_k}{\sum_k P(\tau_k)} \tag{5}$$

and

$$\overline{\tau^2} = \frac{\sum_k P(\tau_k)\tau_k^2}{\sum_k P(\tau_k)} \tag{6}$$

This delay spread determines the maximum bit rate that is achievable for the wireless communication channel. If the symbol period is shorter than the delay spread, the symbols will overlap each other and Inter Symbol Interference (ISI) appears, which disturb the symbols. So the symbol period should be larger than the delay spread to overcome ISI. And that puts an upper limit to the achievable bit rate.

The frequency-reciprocal of the delay spread is called the *coherence bandwidth*: the bandwidth over which the channel is called flat (received power not changing more than 3 dB). If the signal bandwidth is greater than the coherence bandwidth (which is the case with a wideband signal), the channel is called frequency selective: different frequencies cause different fades.

The time-variant nature of the channel can be described by the *coherence time*. The coherence time is the time over which the channel is assumed to be constant. The frequency reciprocal of the coherence time is called the *Doppler spread*: a figure for the shift (spread) of the frequency caused by the change of the channel in time.

# 2. Measurements

As described earlier a good understanding of the radio propagation is crucial for the development of a good mobile communication system. To make a first impression of the wireless communication channel at 60 GHz at different environments, some channel measurements in the frequency domain were performed.

## *2.1 Setup*

Measurements were performed in the frequency domain (simplified swept frequency measurements), for several reasons:

- we were interested in the wideband characteristics, especially the frequency selective fading for an OFDM system
- some equipment was already available
- it was not difficult to use (good transportable)

The main interest was to measure the wideband characteristics of different environments, both indoor and outdoor. These wideband characteristics are not known for 60 GHz and are very important for a modulation technique like OFDM (Orthogonal Frequency Digital Multiplexing) with its multiple carrier-components, which is a very promising candidate for MBS.

The block diagram of the measurement system used for the frequency-domain characterization of the radio-channel is shown in *Fig. 1*. The used equipment was:

- synthesized signal generator (Marconi 2024)
- NEC 60 GHz transmitter (8PSK)
- NEC 60 GHz receiver (8PSK)
- Spectrum analyzer (Anritsu MS2651A)
- GP-IB card and Labview software (National Instruments)
- Laptop PC (Compaq Armada 1580 DT)

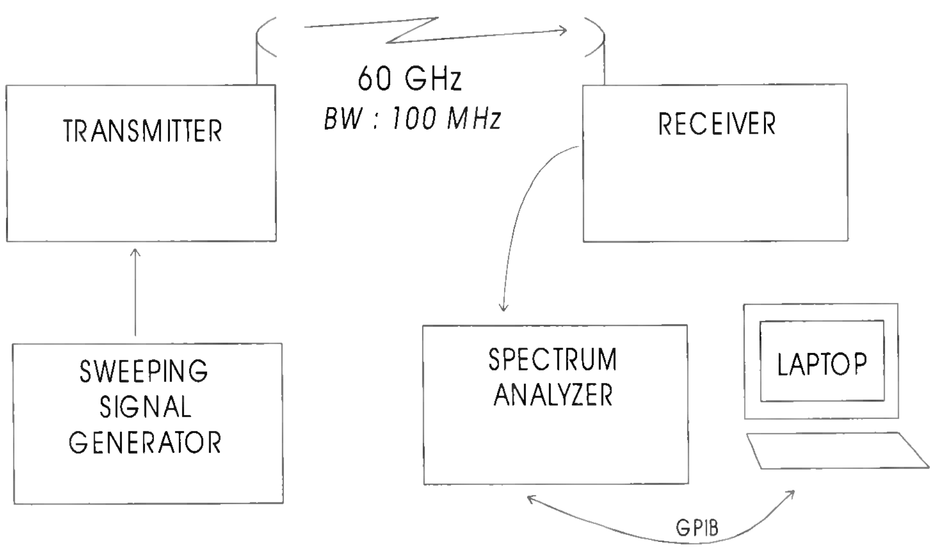


*Figure 1* - Wideband measurement setup

The two main components are the synthesized signal generator and the spectrum analyzer. The CW signal generated at the signal generator (strength: -15 dBm) is fed directly to the intermediate frequency (IF) of the transmitter. The output of the RF power amplifier is radiated through an omni-directional antenna. The energy collected at the receiver antenna (omni-directional or directional) is translated to the IF of the receiver. That signal is fed to the spectrum analyzer to determine the frequency response of the channel. From the spectrum analyzer, data was transferred to a laptop PC via GPIB (General Purpose Information Bus) and stored for later analysis. On the laptop PC a measurement software tool (Labview) was installed. By writing special Labview programs that controlled the spectrum analyzer, most of the measurements were done automatically. But because there was no synchronization with the signal generator, the measurements could not be done completely automatically.

The frequency response consists of 500 power samples at a frequency spacing of 0.2 MHz, as shown in *Fig. 2*. For each point, the distance was also measured.

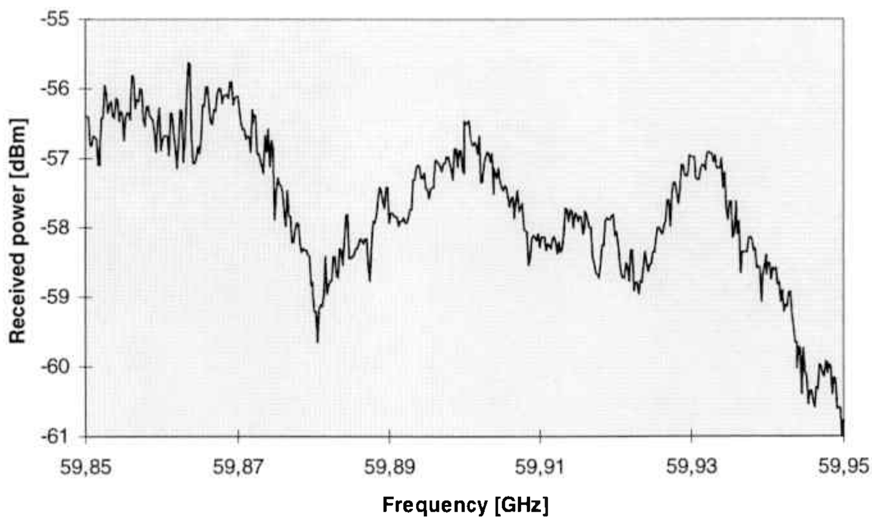


*Figure 2* - An example of a frequency response measurement made with the spectrum analyzer (the magnitude in [dBm])

At the transmitter side was used a flat omni-directional antenna (2dBi, 120°). At the receiver side, we had the choice between an omni-directional (120°) or a patch directional antenna (pencil beam, 19.5 dBi, 15°, gain of 15 dB). The antenna diagrams of the omni-directional transmitter antenna, omni-directional receiver antenna and directional receiver antenna are given in *Fig 3,4,5*. Measurements with both were done in order to see the difference of receiver performance, because an omni-directional antenna allows for more reflected components to enter the receiver.

The measurements were done over a range of distances. Every measurement the receiver was shifted manually one step further in the distance range. For one situation rails were used to move the receiver. The rails allow automatic (computer controlled) measurements with a precision of 1/20 mm. The rails consist of a cart moved along the 10 m rail, by a step motor controlled through a RS232 interface. The rails are constructed in such a manner that it is reconfigurable for different antennas and instruments. Also, it is easily moved for measurements in different locations.

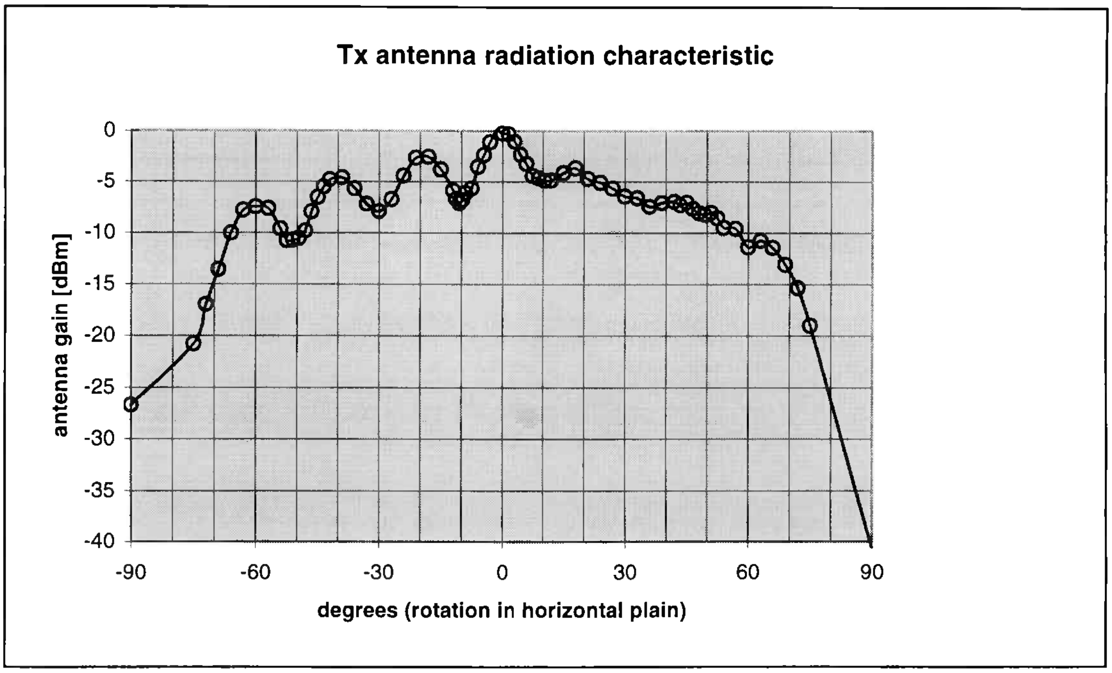


*Figure 3* - Antenna diagram of the omni-directional transmitter antenna

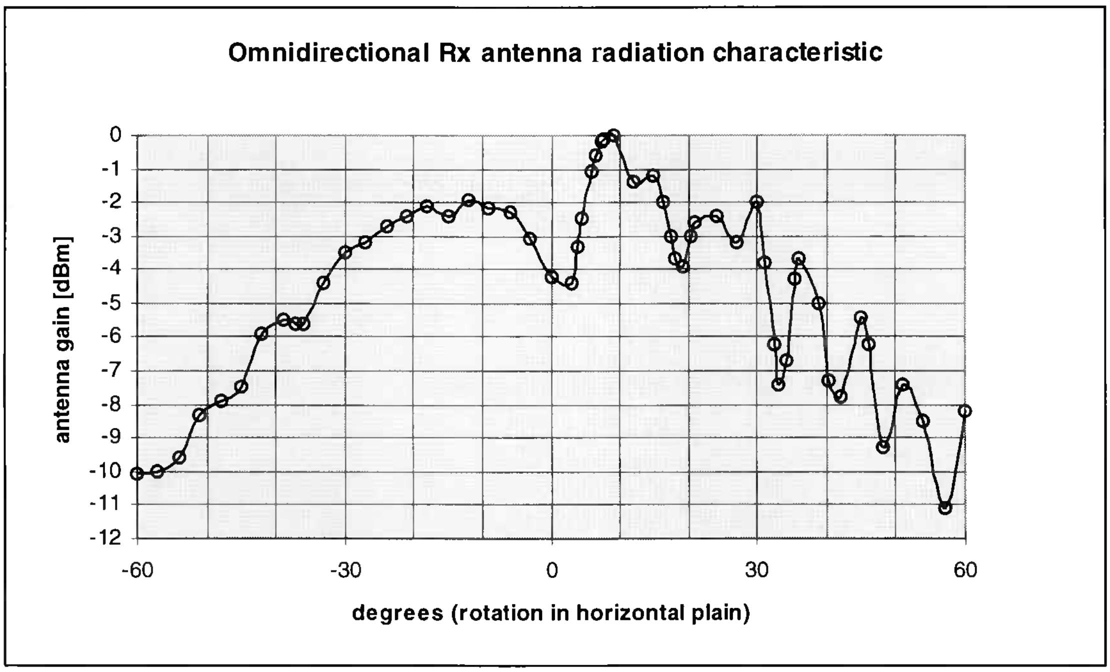


*Figure 4* - Antenna diagram of the omni-directional receiver antenna

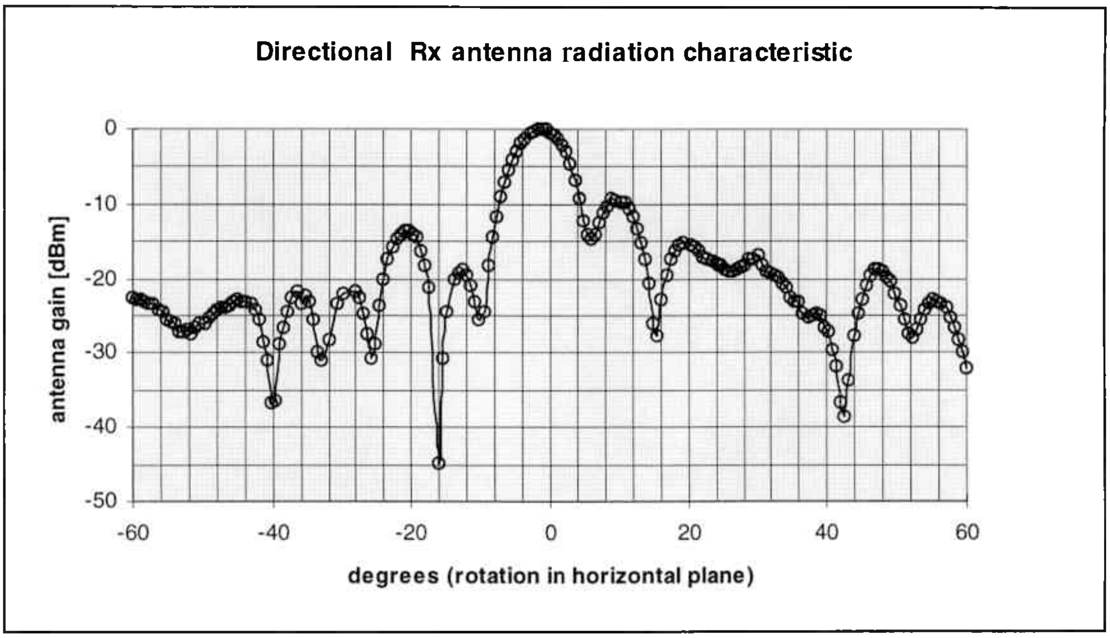


*Figure 5* - Antenna diagram of the directional receiver antenna

There were two types of measurements:

- CW (carrier wave)
- wideband (100 MHz bandwidth)

The measurements were done in the Faculty of Electrical Engineering and around it in the campus of the TU Delft. Environments investigated were (indoor and outdoor):

CW measurements in the corridor and a room on the 19th floor.
Wideband measurements at the:

- corridor on the 19th floor,
- big college room A (amphitheater),
- grassfield at the side of the EE building,
- parking on the back of the EE building.

## *2.2 Carrier Wave measurements*

### 2.2.1 Corridor

In order to see what kind of effect an environment like a corridor has on the path loss, CW measurements have been carried out in the corridor on the 19$^{th}$ floor at the Faculty of Electrical Engineering of the TU Delft.

For the CW measurements the Carrier Frequency in the signal generator was not swept, but held constant at the central IF (intermediate frequency) of 1900 MHz.

A sketch of these measurements is given in *Fig. 6*. The antenna heights were 1m84. They were positioned in the middle of the corridor and pointed towards each other. Both antennas were omni-directional. The antennas were standing still while measurements were done, in order to keep the channel constant.

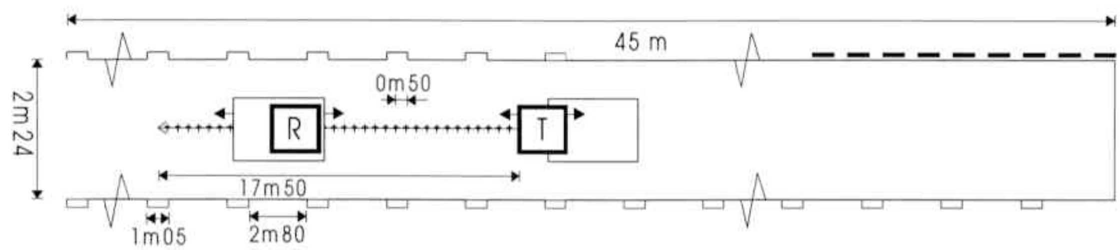


*Figure 6* - CW measurements in the corridor (from 0.5 m to 17.5 m)

At each position the received peak power (in dBm) was averaged 10 times and then stored in the laptop as a measurement sample.

The measurement samples were taken at different distances between transmitter and receiver antenna, from 0m49 until 17m51. Every 0.5 m, 9 samples were taken, with the distance of 2.5 mm between these samples 2.5 mm. For example, around 0.5 m the sample-locations were: 0m49, 0m4925, 0m4950, 0m4975, 0m50, 0m5025, 0m5050, 0m5075 and 0m51.

For the final graph of received power against distance (*Fig. 7*) these 9 samples were averaged and resulted in a local average received power. Finally, we get a graph of 35 local averages.

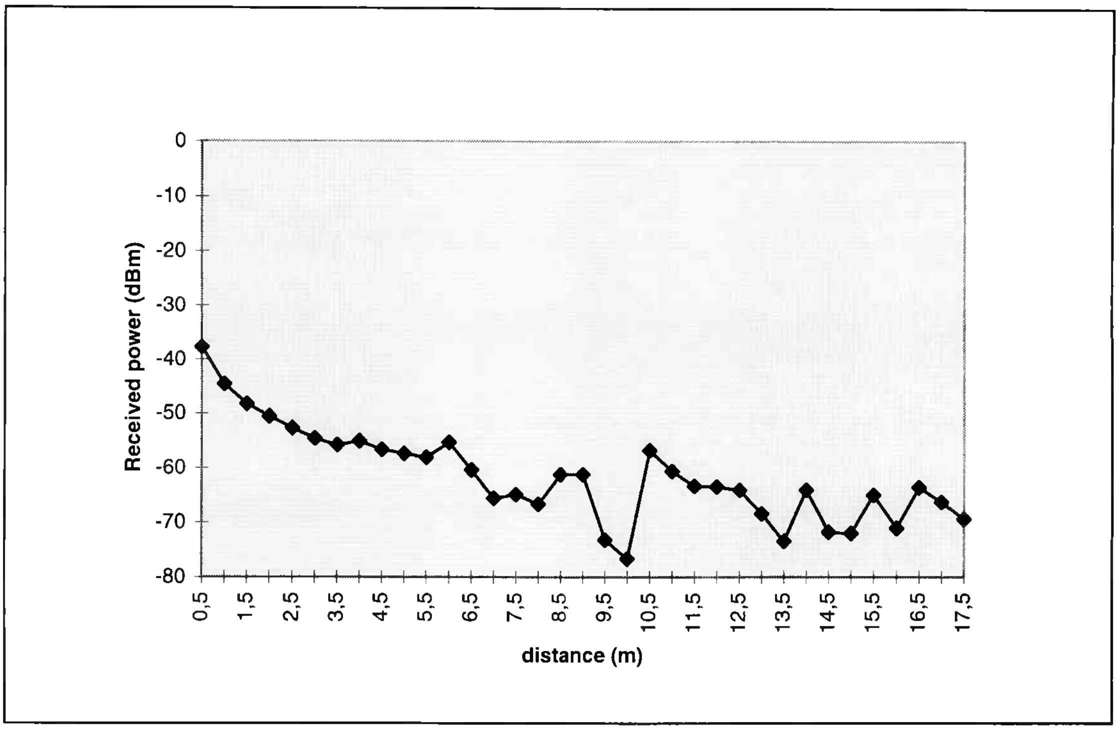


*Figure 7* - CW measurements at the corridor from 0.5 m until 17.5 m in steps of 0.5 m

From this graph, we can see that until 5 m the signal monotonously decreases, but then starts to fluctuate a lot. This is a result of large-scale multipath effects. After 5 m distance between the transmitter and receiver antenna, the reflections of the walls start to play a significant role and therefore multiple rays get inside the receiver antenna and interact with each other. It is also seen that the average signal is not decreasing so fast after 5 m as before that. That can be explained by the fact that the signal stays within the corridor, i.e. the corridor behaves as a waveguide.

To see the effects of path loss and multipath fading for a CW on a small scale of this distance range, CW measurements were also performed with a rails in the distance range of 6-7 m and a step size of 1 mm. The rail allows minimum steps of 1/20 mm. This minuscule step is very important as it gives a possibility to access changes of the field in the millimeter wave range, for instance on the 60 GHz the wavelength is only 5 mm. Again, both antennas were omni-directional.

The results of these measurements are plotted in *Fig. 8*. This figure shows that the received signal is very sensitive to small distance shifts. Even within a wavelength (which is only 5 mm) deep fades can occur. That shows the importance that the multipath fading effect has on the overall propagation, especially the small-scale multipath fading.

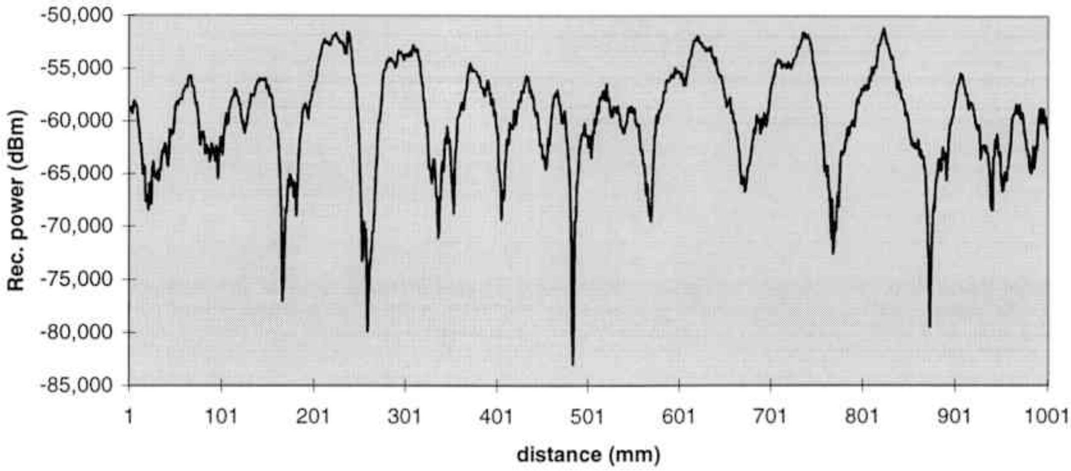


*Figure 8* - Rec. power versus distance from 6 to 7m in steps of 1mm

### 2.2.2 Moving with receiver antenna

To see the effects of a moving antenna, some measurements were performed while walking with the receiver antenna, once in the corridor, once in a room.

While continuously slowly walking away and moving the receiver antenna to the left and right side of the corridor every second a sample was taken of the received power at a distance range of 80 cm until 24 m. The total time taken was 7 min, so the speed of walking was about 5cm/ s. In *Fig. 9* the resulting figure is shown. From this figure it can be seen that the received power of the mobile terminal is also very sensitive to motions and can cause strong fluctuations.

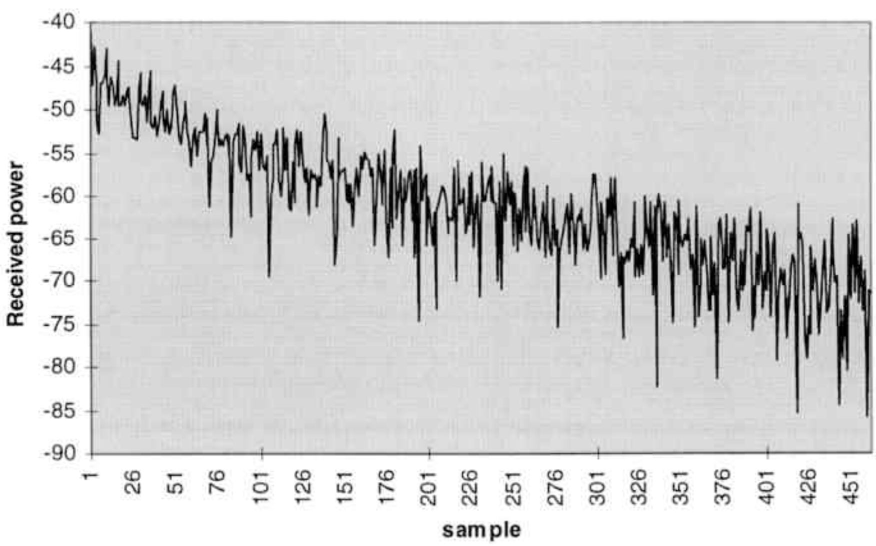


*Figure 9* - CW measurements with a moving omni-dir. receiver antenna from 0,8 to 24 m in the corridor

In a room a similar kind of measurement was done, but now with the transmitter antenna just under the ceiling and the omni-directional receiver antenna on a movable car. This time during 20 min. 4 different circles around the room were walked without sweeping the receiver antenna left or right.
Both for the corridor and the room the antennas were more or less pointing at each other. The resulting figure for the room is given in *Fig. 10.* Again is seen that the position of the moving receiver antenna can have a strong impact on the received power.

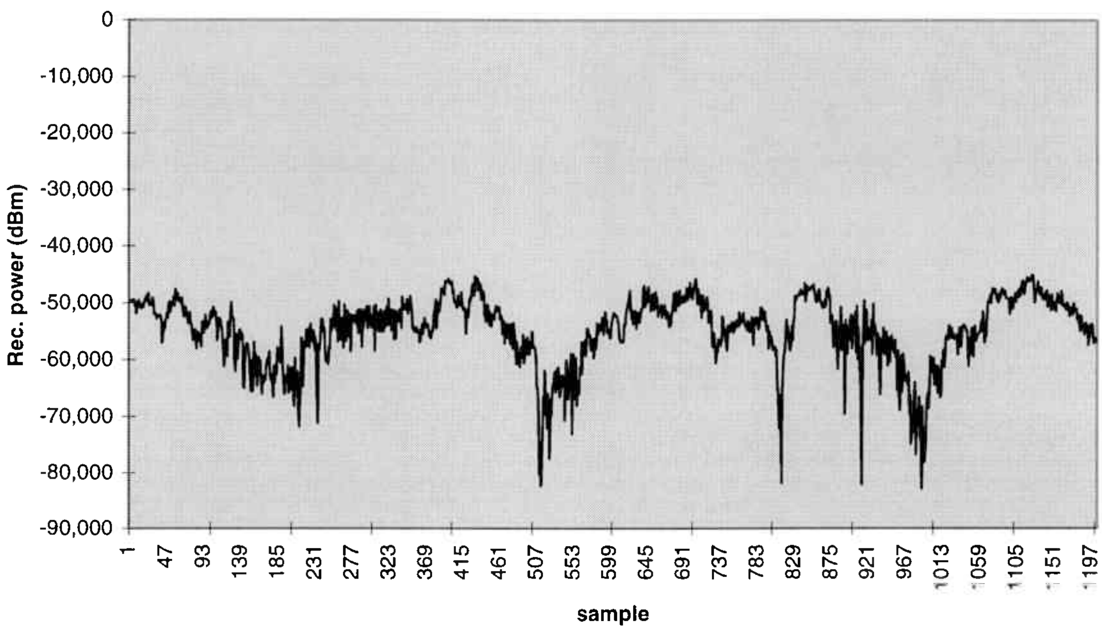


*Figure 10* - CW measurements with a moving receiver antenna in the room

### 2.3 Wideband measurements

In order to get samples of the spectrum the first step was to automate the measurements, because they can not be done with hand. A screen of the spectrum analyzer that was used had 500 points and each one of them has a value associated with it. Thus, each point mentioned in the further text was put in a file consisting of 500 numbers plus general log information, such as date, time, etc. 500 points were enough to cover the bandwidth accurately.

Since the goal of this kind of measurements is to get a statistical distribution of the small-scale fading (Rice factor), it was interesting to record many points with different properties.

For the wideband measurements the Carrier Frequency was swept at the signal generator with a step of 200 kHz, every 200 ms, from 1850 MHz to 1950 MHz. In the transmitter the signal was converted up to 59.9 GHz and at the receiver converted back to an IF of 140 MHz. The maximum values of the signal from the receiver were held at the spectrum analyzer with a bandwidth of 100 MHz. When the complete bandwidth of 100 MHz was swept, the measurement data were stored in the laptop and one of the antennas was moved to the next point of interest and the next measurement was done. The bandwidth was taken as 100 MHz, because the antennas were known to be operating well in this frequency region.

The rails were not available at the time of measurements, so the question was how dense should the measurements be done, because the moving of the antenna had to be done manually and was not very precise. An experiment was done to determine that. First, the spectrum was measured with 2 omni-directional antennas with a step of 2.5 mm, which is half wavelength on the 60 GHz. The result is presented on the *Fig. 11*. It can be seen that there is a large correlation of the spectrum shapes between these points.

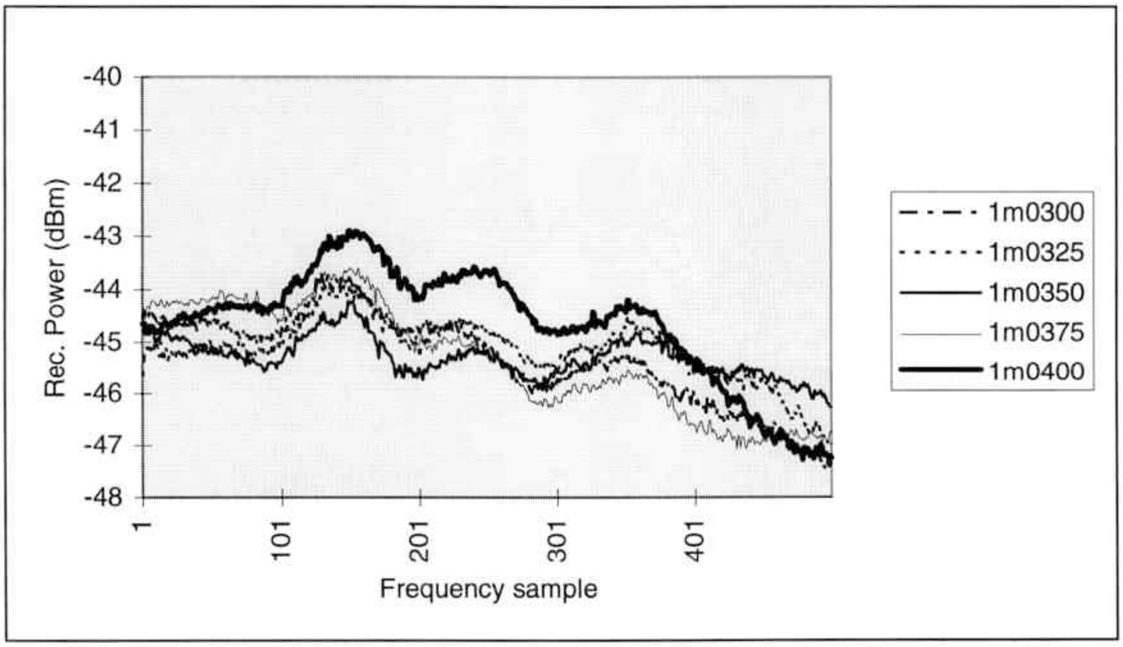


*Figure 11* - Wideband measurements at a room with both omni-directional antennas in steps of 2.5 mm

Because the goal was points with different distribution, the same type of measurement was done again, but this time with a step of 1 cm. This experimental results are given at *Fig 12*. Looking at this graph, one can see that correlation stops at the distance of approximately 4 cm. A final decision was made to take samples in the corridor with that step.

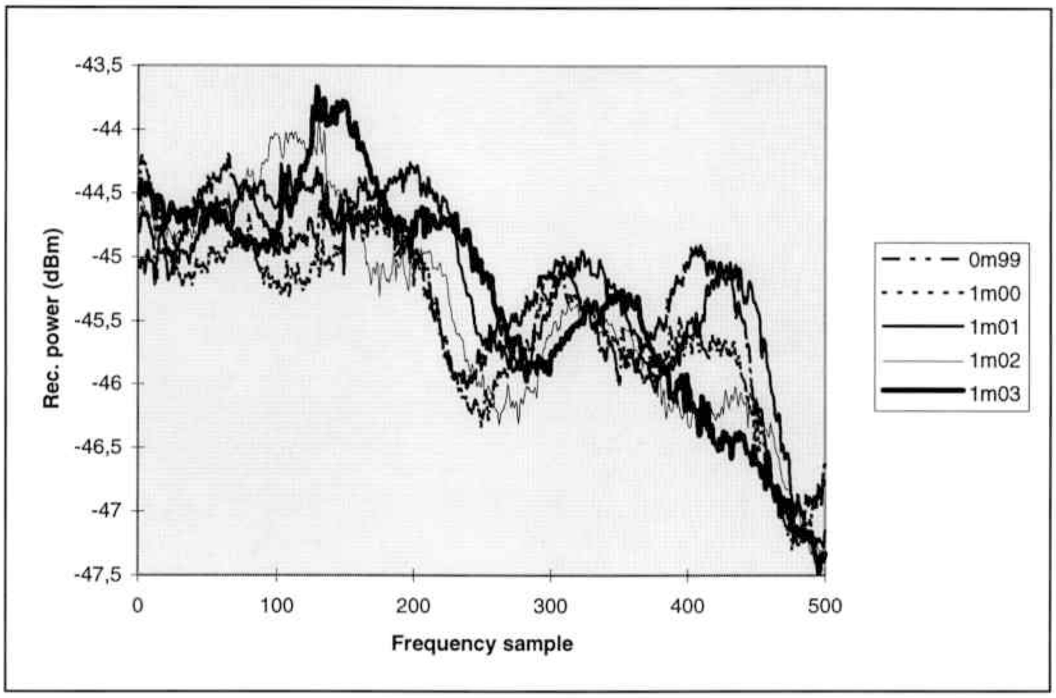


*Figure 12* - Wideband measurements at a room with both omni-directional antennas in steps of 1 cm

### 2.3.1 Calibration

In order to see if the measurement equipment is suitable to measure accurately enough, a few calibration measurements are made (*Fig. 13*). Therefore instead of placing antennas between signal generator and spectrum analyzer, a coax cable of 5m08 is connected between signal generator and spectrum analyzer. It can be seen that the spectrum is not flat, but slowly increasing with something like a wave-pattern, probably a result of some non-linearity's within the equipment. Out of this figure can be concluded that the accuracy of the equipment is around 1 dB (because each calibration measurement is within 1 dB). And although a more detailed description will follow this 1 dB accuracy will be taken in general for the measurements.

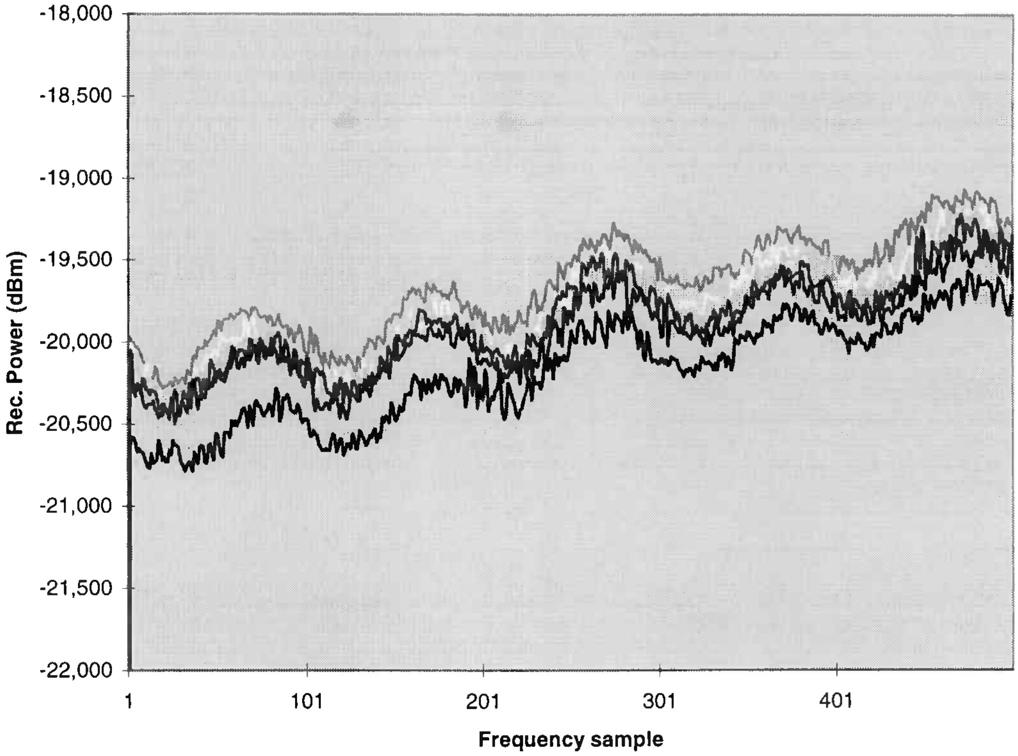


*Figure 13* - Calibration measurements

Looking with more detail to *Fig. 13* it can be seen that the received power is the sum of three components. The first is the expected direct (DC) component from the transmitter and the other two are unwanted delayed components (one causes "fast" frequency fading, one causes "slow" frequency fading), probably caused by a mismatched cable or equipment (reflection) or cross-talk from outside. *Fig. 14* shows a sketch of the two different unwanted components.

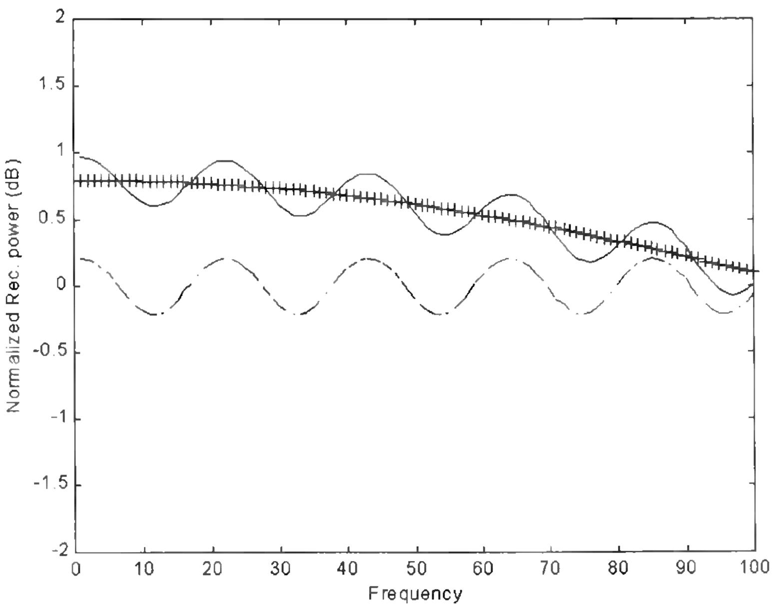


*Figure 14* – Sketch of the 2 different unwanted components (-- = "fast", ++ = "slow") and the combination of both (straight line)

The received power is then defined by these 3 components:

$$|H(jf)|^2 = \left|\sum_{m=0}^{2} \beta_m e^{j(2\pi f\tau_m + \theta_m)}\right|^2 \tag{7}$$

From *Fig. 13* and *Fig. 14* an indication of the amplitudes and delay times (phase information is not interesting in our case) of the different frequency components can be obtained. The slow unwanted component has a relative frequency of about 400 MHz, which if inverted yields a delay $\tau_1$ of 2.5 ns and the amplitude $\beta_1$ is around 0.2 times the amplitude $\beta_0$ of the DC component. The faster unwanted component has a relative frequency of about 20 MHz, which yields a delay $\tau_2$ of 50 ns and the amplitude $\beta_2$ is around 0.05 times the amplitude $\beta_0$ of the DC component. This is plotted in a time delay profile *(Fig.15)*, where the 3 different time components are clearly visible.

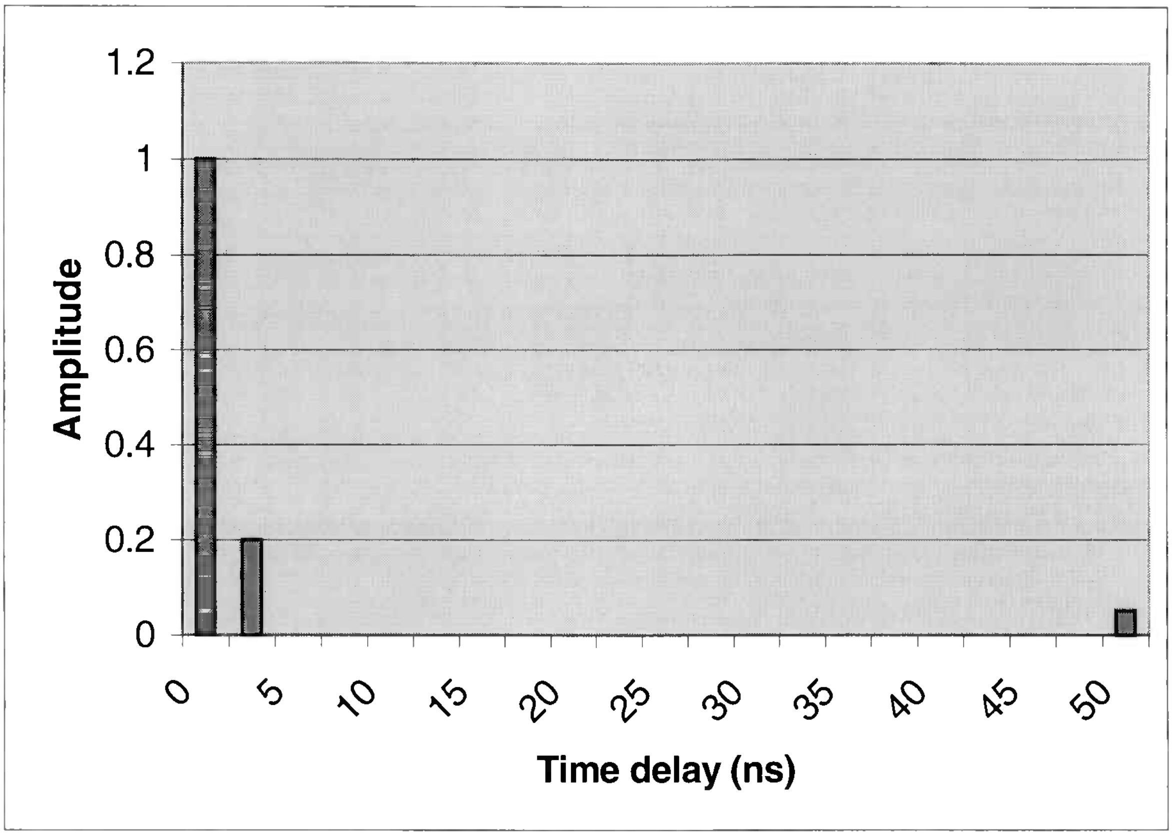


*Figure 15* – Sketch of the Time delay profile of the calibration measurement

## 2.3.2 Corridor

To observe the effects of the corridor on the wideband characteristics of the signal, measurements were done with both the omni-directional and directional antenna. Again the antennas were standing still during measurements.
A sketch of the measurements is given in *Fig. 16*.

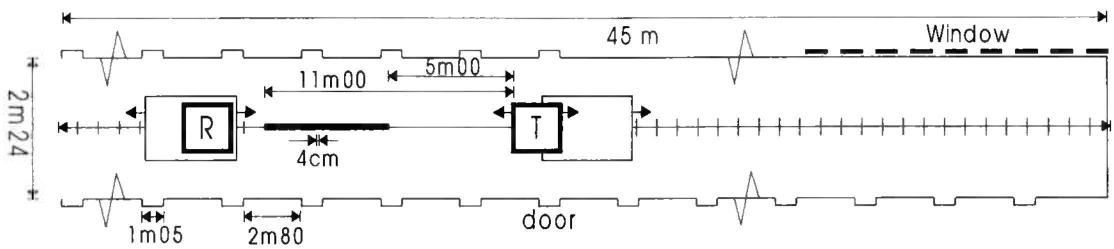


*Figure 16* - Wideband measurements at the corridor, 5-11 m in steps of 4 cm (thick line) and 11-44 m with step of 1 m

At each position a sample of a bandwidth, 100 MHz broad, was measured and then stored in the laptop as a separate file. For both receiving antennas the measurements were taken from 5m00 until 11m00 in steps of 4 cm to see the effects in small distance differences. The effects for bigger distance differences were observed by measuring every meter, for the omni-directional receiver antenna from 11m00 until 43m00 and for the directional receiver antenna from 11m44 until 43mm44.

Examples of the measured spectrum for both the omni-directional and directional receiver antenna are given in *Fig. 17, 18.*

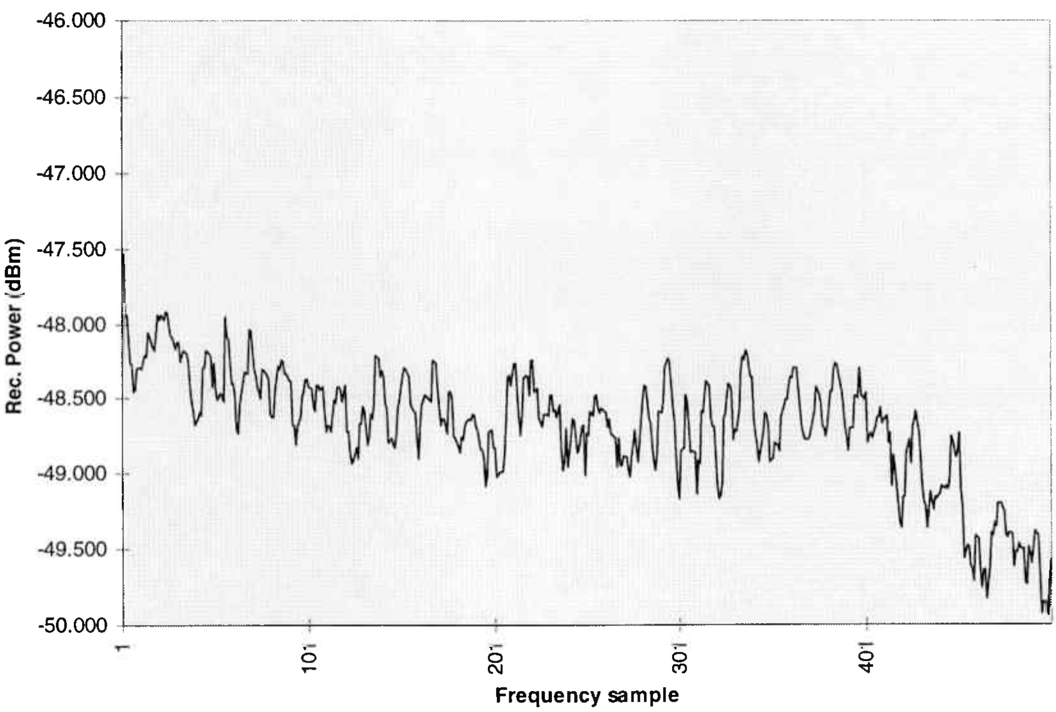


*Figure 17* - Sample of measured spectrum in the corridor with directional receiver antenna

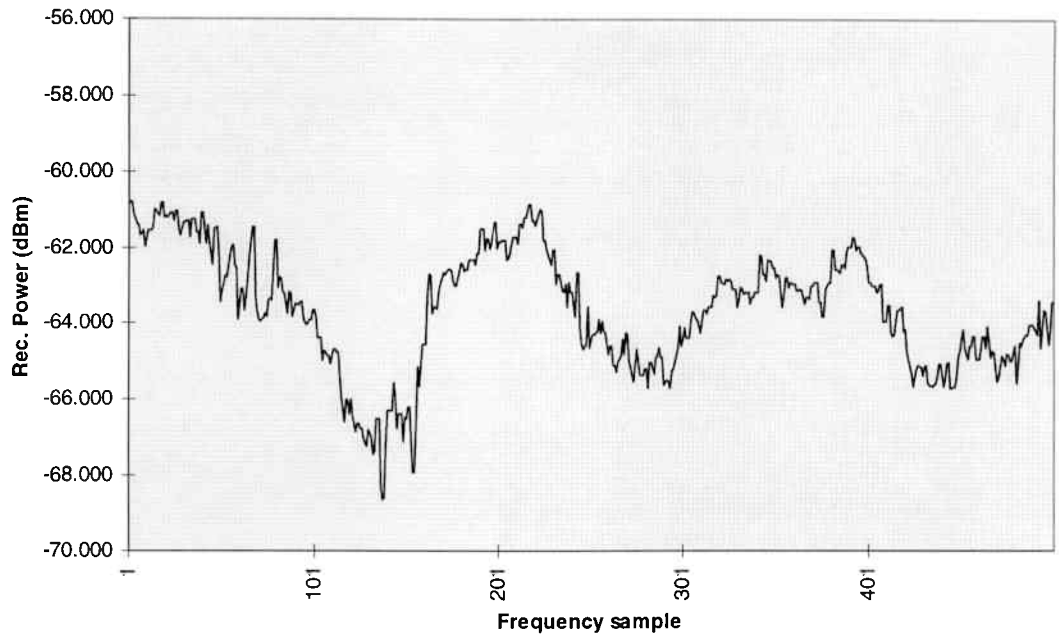


*Figure 18* - Sample of measured spectrum in the corridor with omni-directional receiver antenna

From the measurement observations (the spectrum for directional antenna was almost flat unlike the spectrum of the omni-directional which was more fluctuating, see *Fig. 17,18*) it was clear that for the directional receiving antenna the multipath effect is much less than for the omni-directional antenna. Only for distances of more than 30 m the multipath become visible for this antenna in terms of a more fluctuating spectrum. The reason is the much narrower antenna bundle for the directional antenna that causes the first reflections from the wall to be received only from 30 m. Also the waveguide-effect made it possible to receive quite a good signal at the end of the corridor (distance of 44 m), although some part of the spectrum reached the noise level (-90 dBm).

Another observation was the effect of people. When people were walking through the corridor, usually there was no drastic change of the received signal. Only when somebody crossed the Line-of-Sight (LOS), there was a dip in the signal, with directional antenna a larger one than with the omni-directional antenna. When people didn't walked in the LOS-component there was no effect visible.

### 2.3.3 Amphitheater

To observe the effect of a very large room on the propagation, wideband measurements were taken in the biggest amphitheater of the Faculty of Electrical Engineering building of the TU Delft. The college room has a slope in it. Two kinds of measurements were performed :

1. static transmitter in the lower part of the room and 50 different receiver positions
2. static transmitter in the upper part of the room and 50 different receiver positions

In both situations, the used antennas (transmitter & receiver) were omni-directional. For both kinds of measurements, the transmitter antenna is set diagonally with the same slope as the amphitheater. Every time a measurement was performed, the antennas were pointed towards each other. The height of the transmitting antenna down is 1m70 above the floor. Both situations are sketched in *Fig. 19* and *20,* respectively.

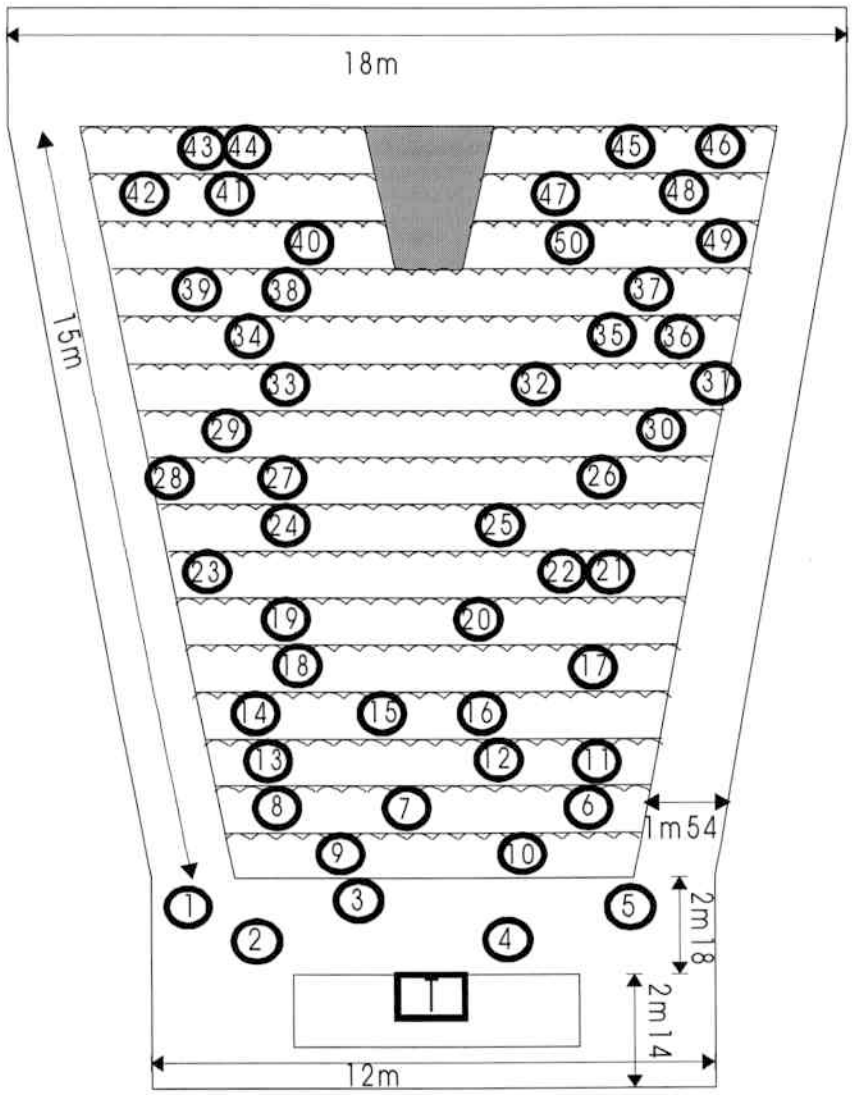


*Figure 19* - Wideband measurements on 50 receiver (omni-directional antenna) positions with transmitter down at college room A

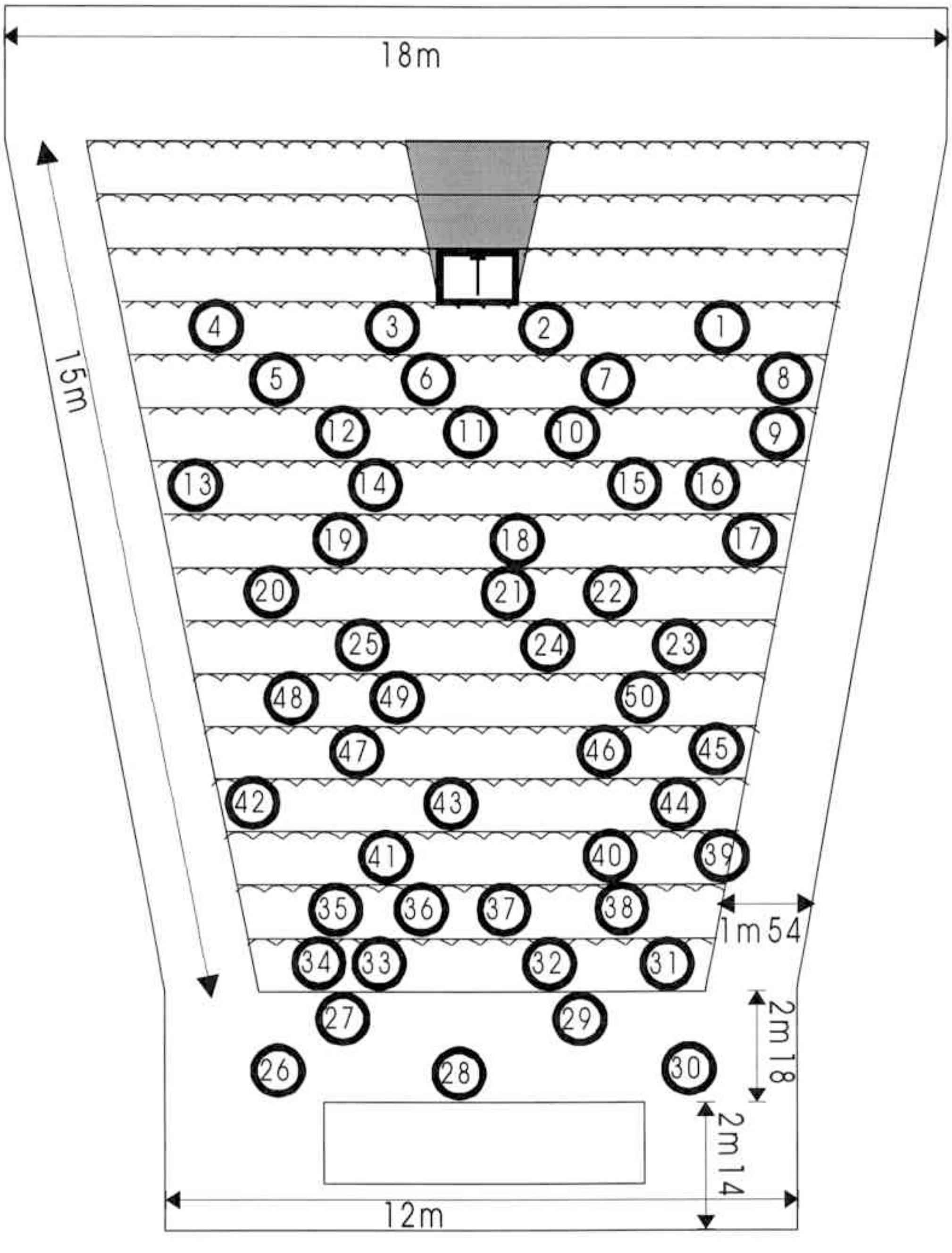


*Figure 20* - Wideband measurements on 50 receiver (omni-directional antenna) positions with transmitter up at college room A

These experiments are interesting for evaluation of communication possibilities in large lecture halls, airport lobbies or factories. Observations from the measurements (*Fig. 21*) showed that the impact of multipath was less than in the corridor. That was expected, since the reflection walls were further away. And the multipath effect is stronger at the sides of the amphitheater than in the middle, which is explained by the fact that the walls of the amphitheater play a role as reflection wall.

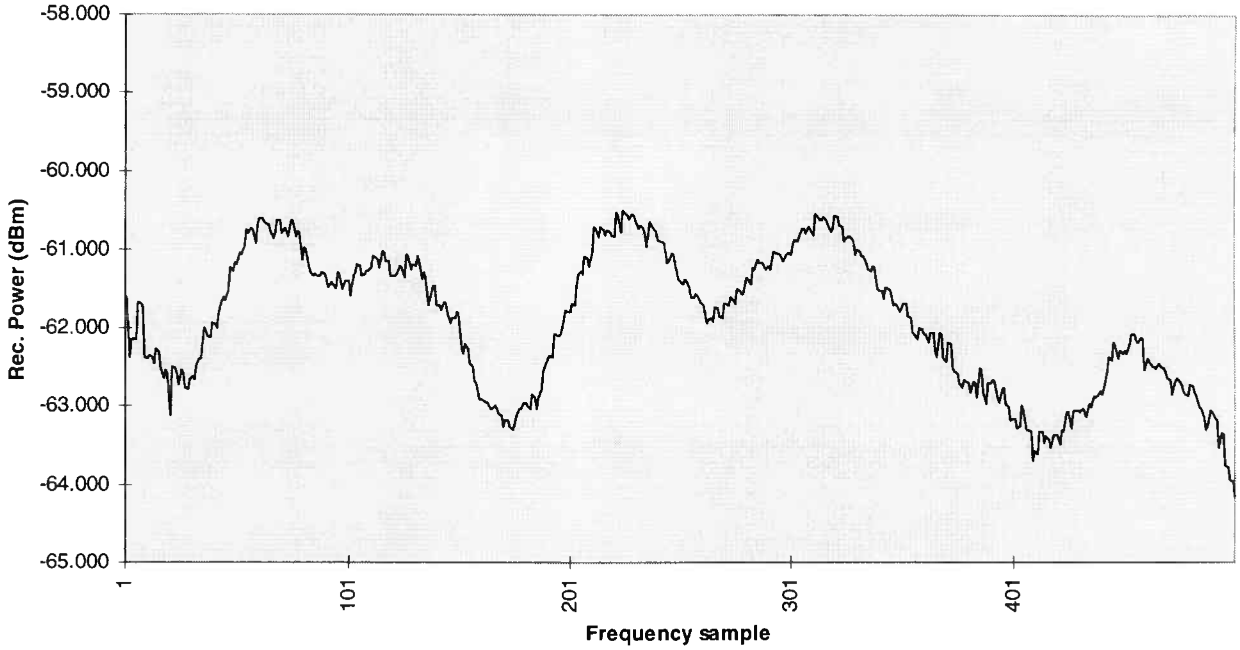


*Figure 21* - Example of measured spectrum at the amphitheater

### 2.3.4 Outdoor

To see if there is a difference between an indoor scenario and an outdoor scenario (for example as a consequence of weather conditions), measurements have also been performed outside the Faculty of Electrical Engineering building, namely at:

- the side of the building at the grassfield
- the parking at the back of the building

Grassfield

Again both antennas were omni-directional. The height of both antennas was 1m59. The measurements were performed from 1 m until 27 m every meter in a straight line with the receiver moving away (but standing still while measuring). A sketch of the complete situation is given in *Fig. 22.*

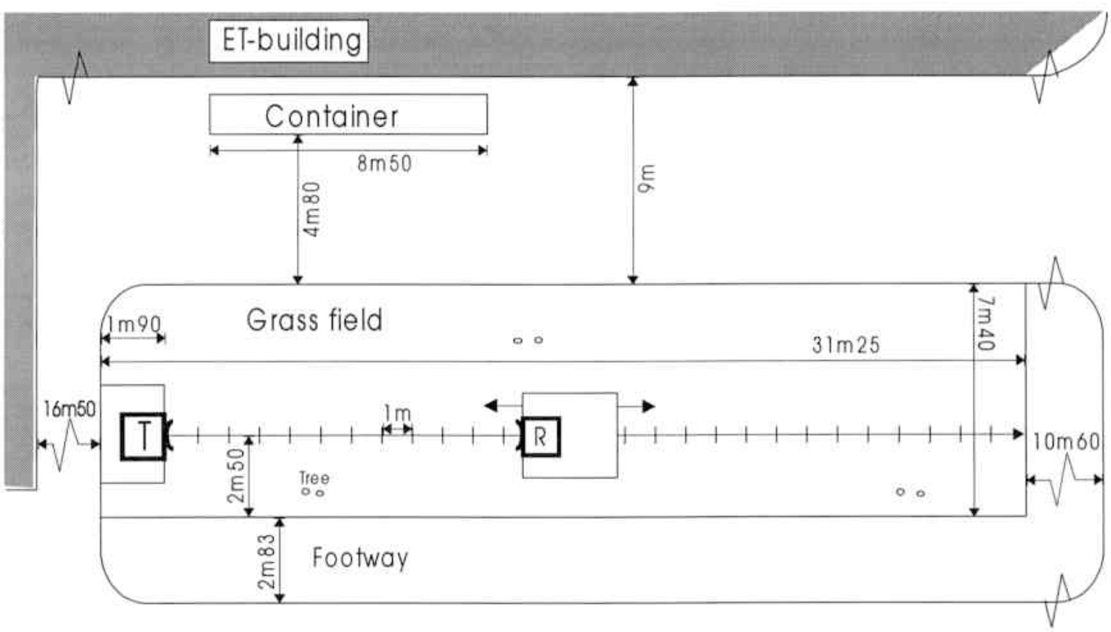


*Figure 22* - Wideband measurements with omni-directional antennas in a straight line at the grassfield

The weather conditions on the time (afternoon) of the measurements were:

- temperature: ± 5 C°
- strong wind
- dry / not cloudy

## Parking

Four kinds of wideband measurements were performed at the parking:

1. In a straight line with omni-directional receiver antenna
2. In a straight line with directional receiver antenna
3. Random 12 positions with omni-directional receiver antenna
4. Random 15 positions with directional receiver antenna

*1. & 2. In a straight line with omni-directional & directional receiver antenna*

The same kind of measurements as on the grassfield were made (in a straight line), only now on the parking and with both receiving antennas: the omni-directional and the directional one. Again, the height of the antennas was 1m59.
For the omni-directional antenna, wideband measurements were made from 2m20 until 26m20 at every meter.
For the directional antenna, wideband measurements were made from 3m20 until 24m20 at every meter.
A sketch is given in *Fig. 23.*

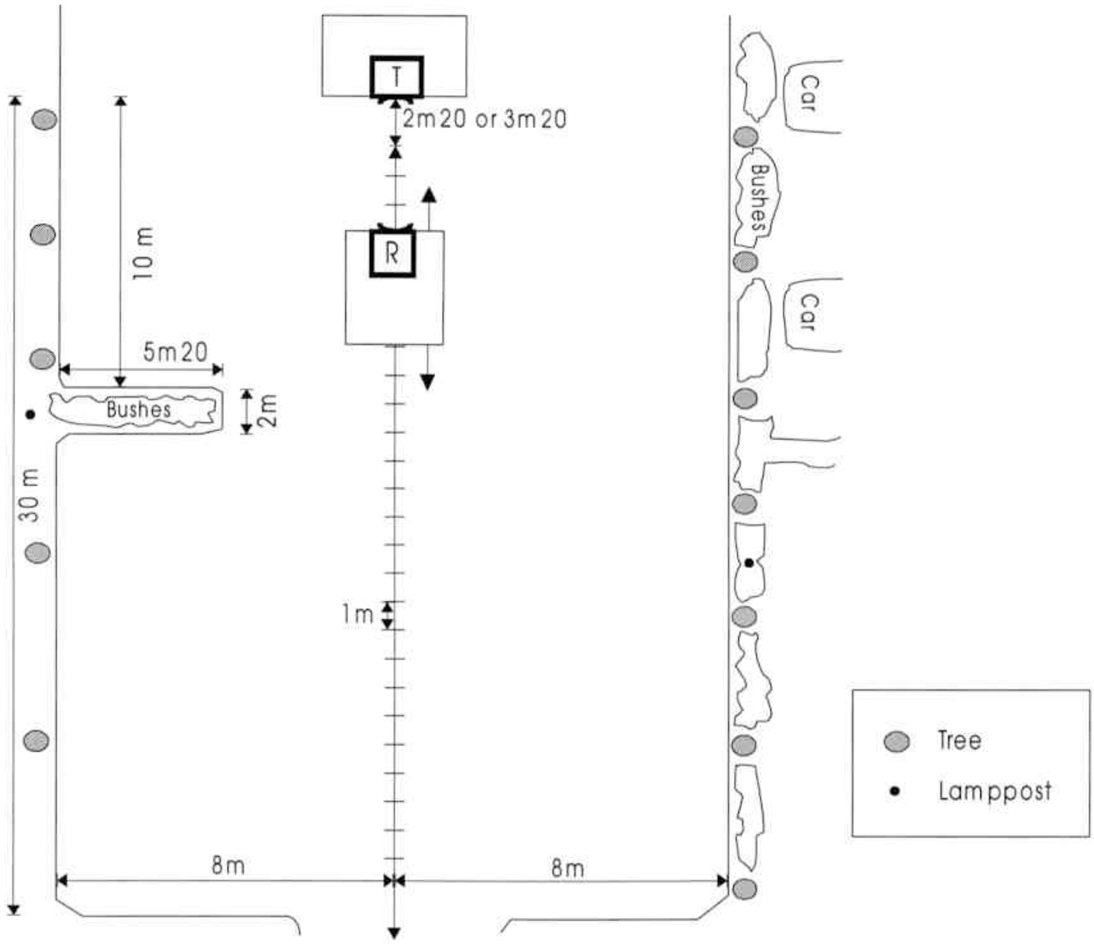


*Figure 23* - Wideband measurements in a straight line at the parking

The weather conditions were:

with the omni-directional antenna :
- temperature : ± 3 C°
- a little windy
- dry / not cloudy
- night

with the directional antenna:
- temperature: ± 5 C°
- windy
- dry / not cloudy
- day

2. *Random 12 positions with omni-directional receiver antenna*

Twelve random positions at the parking were measured to cover the whole parking. The omni-directional receiving antenna was used and positioned just like the transmitter antenna 1m59 above the ground. Both antennas were turned towards each other in every single measurement. The parking was covered with leafs (it was autumn). A sketch is given in *Fig. 24.* The distances between the two antennas are given in the sketch.

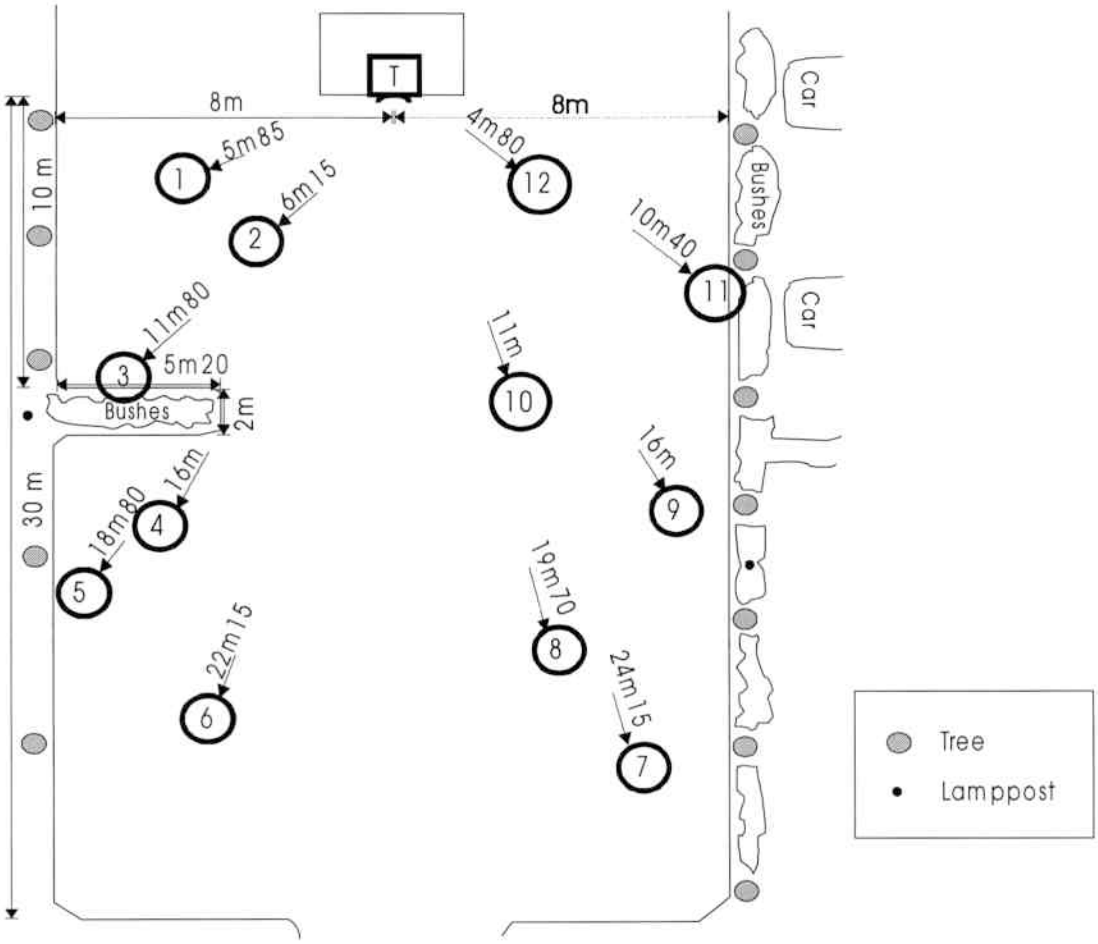


*Figure 24* - Wideband measurements on 12 receiver (omni-directional antenna) positions at the parking

The weather conditions on the time (afternoon) of the measurements were:

- temperature: ± 5 C°
- strong wind
- dry / not cloudy

*3. Random 15 positions with directional receiver antenna*

The same situation as described before, but now with the directional antenna and 15 random positions at the parking were chosen to cover the whole parking. A sketch is given in *Fig. 25.* The distances between the two antennas are given in the sketch.

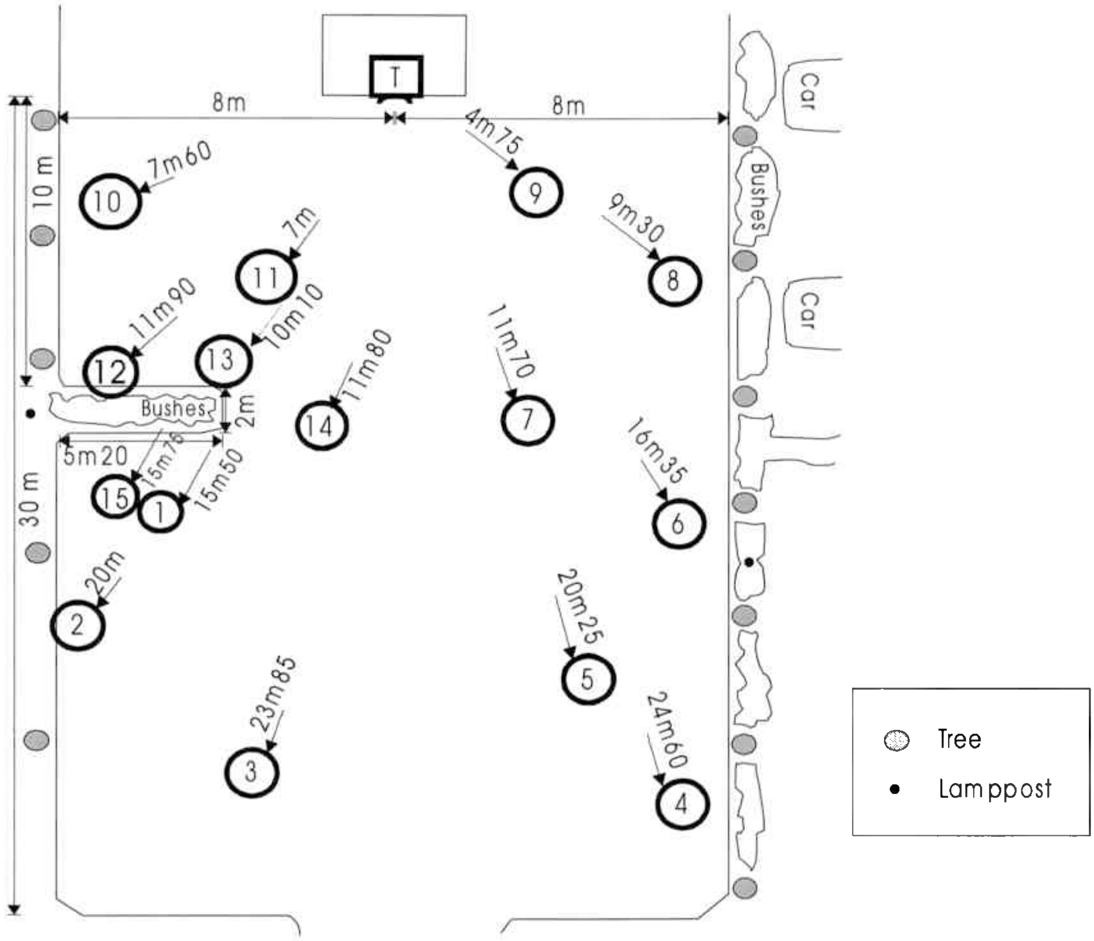


*Figure 25* - Wideband measurements on 15 receiver (directional antenna) positions at the parking

The weather conditions on the time (afternoon) of the measurements were:

- temperature : ± 5 C°
- slightly windy
- dry / not cloudy

Also tried is to measure in the rain to see the effect of rain, but unfortunately the weather was not cooperating.
Observations of the measurements show that when the receiver antenna is behind the bushes the received signal-level drops a lot, 20 dB, for both omni-directional and directional antenna. But when the bushes are not very dense, the LOS component can come through and no signal-level drop is visible.

Examples of outdoor measured spectra are given in *Fig. 26.* The two upper lines are examples of measurements with a directional antenna (one in a straight line, one at a random position of the parking). The three bottom lines are examples of measurements with an omni-directional antenna (one at the grassfield, one in a straight line and one at a random position of the parking).

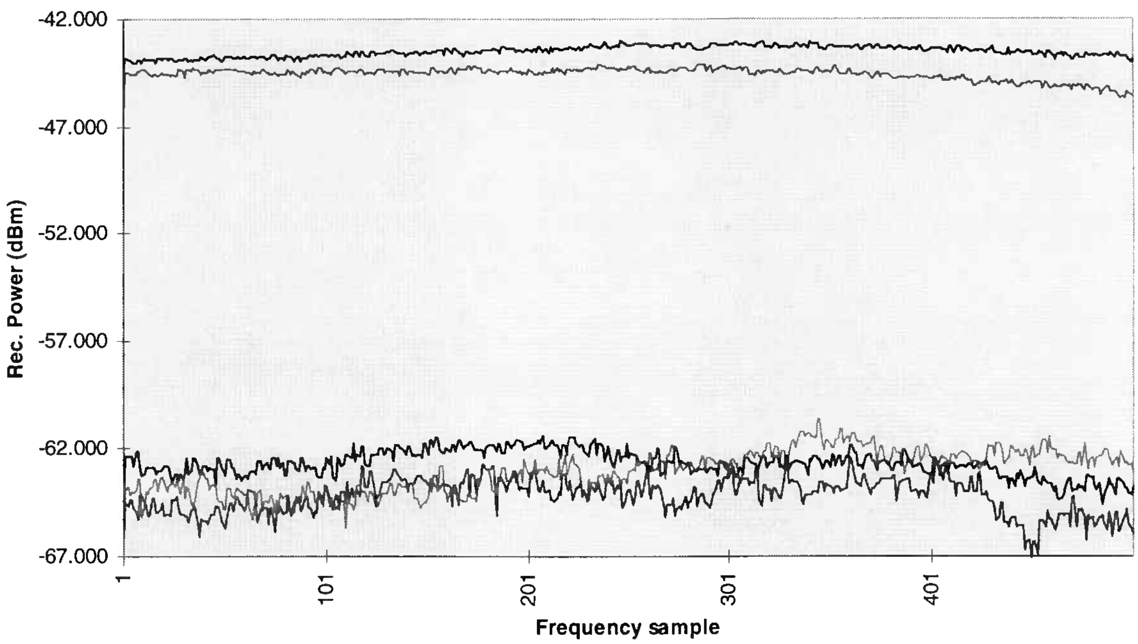


*Figure 26* - Wideband measurements outdoor (with both omni-dir. and dir. receiver antenna)

As one can see, there is not much difference in these measurements and the omni-directional outdoor measurements are quite flat, so it appears that multipath doesn't play a significant role. That is understandable, because there were no major obstacles or reflection walls in the measured outdoor environment. Even a difference between measurements in a straight line and at spread positions is not visible. The difference between the directional and omni-directional measurements are in the order of the gain of the directional receiver antenna, namely 15 dB.

It doesn't appear that weather conditions like temperature and wind play a role in the propagation, but the question if rain could influence the channel remains unanswered.

# 3. Measurement analysis

Part of the measurement analysis was already done in the chapter "Measurements" itself by analyzing the power spectra that were measured. However, a more thorough analysis can be made. Parameters that can describe the wireless communication channel like path loss factor, K Factor, delay spread or coherence bandwidth are extracted from the measurements and the methods to do that will be described here.

Because only the amplitude of the received power was measured (there was no information about the phase or delays), not every detail can be extracted from the measurements. As said before, a complete description of the wireless multipath channel can be made by the complex impulse response model, but that requires information about the phase and delays. However, with the power measurements made for this research good indications can be made to obtain a global description of the transmission channel.

For the measurements a static channel was assumed (receiver and transmitter antennas were standing still, as well as the environment), so time-varying aspects were neglectable. The channel can be seen as a frequency selective, slowly fading channel.

From the CW and the wideband measurements the path loss factor can be extracted. The K-factor, coherence bandwidth and delay spread are extractable from the wideband measurements.

Environments are denoted by:

- I1: Corridor (Indoor)
- I2: Amphitheater (Indoor)
- O1: Grassfield (Outdoor)
- O2: Parking (Outdoor)

### *3. 1 Rice factor K*

Because there was always a LOS path present, the Rician distribution [4, Ch.3 and 4] can be applied as the probability distribution function for the small-scale fading multipath received signal amplitude. The sum of the direct and reflected waves can be expressed as follows in time and frequency domain:

$$h(t) = \sum_{m=0}^{N} \beta_m e^{j\theta_m} \delta(t - \tau_m) \xleftrightarrow{FT} H(f) = \sum_{m=0}^{N} \beta_m e^{j(2\pi f \tau_m + \theta_m)} \tag{2}$$

where $\beta_m$ is the amplitude gain, $\theta_m$ is the phase, $\tau_m$ is the time delay of the $m$th signal reflection. The spectrum analyzer can measure only the power of the reflected signal P(f) = $|H(f)|^2$. The average received power is given by:

$$\overline{P(f)} = \overline{|H(f)|^2} = \sum_{m=0}^{N} \beta_k^2 \tag{8}$$

it can be calculated from a wideband measurement as the average of the 500 frequency samples.

Rice parameter $k$ is defined as:

$$k \overset{\Delta}{=} \frac{\beta_0^2}{\sum_{m=1}^{N} \beta_m^2} \tag{9}$$

where $\beta_0$ is the direct path amplitude.
By using (8) and (9) is obtained:

$$\overline{P} = \left(\frac{k+1}{k}\right)\beta_0^2 \tag{10}$$

In this equation there are still two unknown variables. To make a system of two equations, in order to find $k$, the following expression is used

$$\sigma_{P(f)}^2 = \overline{P^2(f)} - \left(\overline{P(f)}\right)^2 \tag{11}$$

where $\sigma_{P(f)}^2$ is the variance of *P(f)*, which can also be extracted from the wideband measurements.
In order to simplify the derivation and solve the system, the assumption was taken that the power of the LOS wave is much stronger than the sum of the powers of reflected waves, because measurements were always done with aligning of the antennas, i.e.

$$\sum_{m=0}^{N} \beta_m^4 \cong \beta_0^4 \tag{12}$$

Using (12) to simplify the solution of (11) gives

$$\sigma_{P(f)}^2 = \frac{2k+1}{k^2}\beta_0^4 \tag{13}$$

From the system of (10) and (13), it is possible to calculate $k$ and $\beta_0^2$. Being the solution of a quadratic equation, there are two roots for $k$, one approximately 0, and the other with a large value. The physical meaning of $k$ was used as a criterion to choose one of them. Since there was always a LOS and one root is always approximately zero, it was assumed that it was the large one. In Appendix I the complete derivation of this method to extract the Rice Factor $k$ is described in more detail.

By processing each measurement data file using a Matlab program (extractk.m, see Appendix II), we get a Rician Factor $k$ for each power spectrum and out of that we can get a mean and standard deviation of the Rician Factor $k$ for each different environment (corridor, amphitheater and outdoor) and different type of receiving antenna (omni- or directional).

*Fig. 27* shows changes of the $k$ factor in the corridor (I1), when the directional antenna was used. Table I summarizes the results of the Rice factor $k$ statistics for every environment.

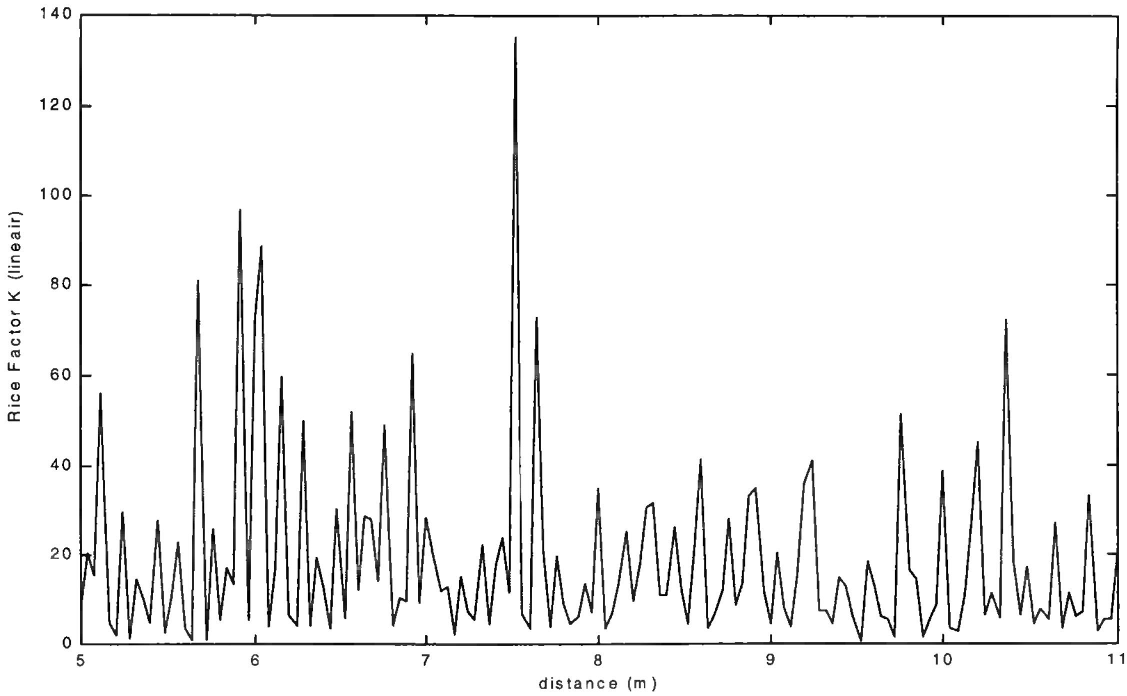


*Figure 27* - Rice factor *k* versus distance in the corridor with an omni-directional receiver antenna used. The *k* scale is (0,140) and the distance step is 4 cm

TABLE I

Average value $\bar{k}$ and standard deviation $\sigma_k$ of Rice factor $k$ over all locations in an experiment environment

| Experiment | $\bar{k}$ | $\sigma_k$ |
|---|---|---|
| I1 (corridor) | | |
| dir. antenna | 169.96 | 101 |
| omni-dir. ant. | 16.79 | 19.38 |
| I2 (large room) | | |
| T up (omni R) | 28.36 | 29.04 |
| T down (omni R) | 56.61 | 78.11 |
| O1 (grassfield) | 84.25 | 87.94 |
| O2 (parking) | | |
| omni-dir. ant. | 80.71 | 79.89 |
| dir. antenna | 423.85 | 165.35 |

To justify the found K-Factors, they have been compared to another method for K-extracting using a fit of the measured cdf with a theoretical cdf based on the K-factor [10,11]. The comparison shows very good agreement *(Fig. 28)*, just like the theoretical and measured cdf *(Fig.29)*.

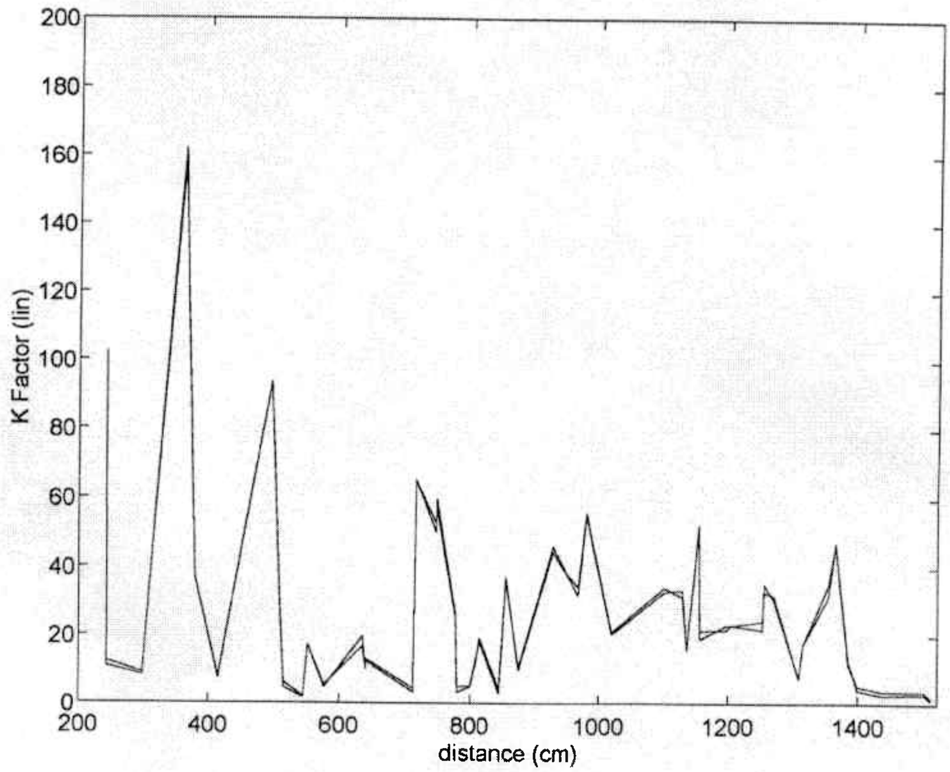


*Figure 28* - Comparison of K Factor Extraction for the amphitheater

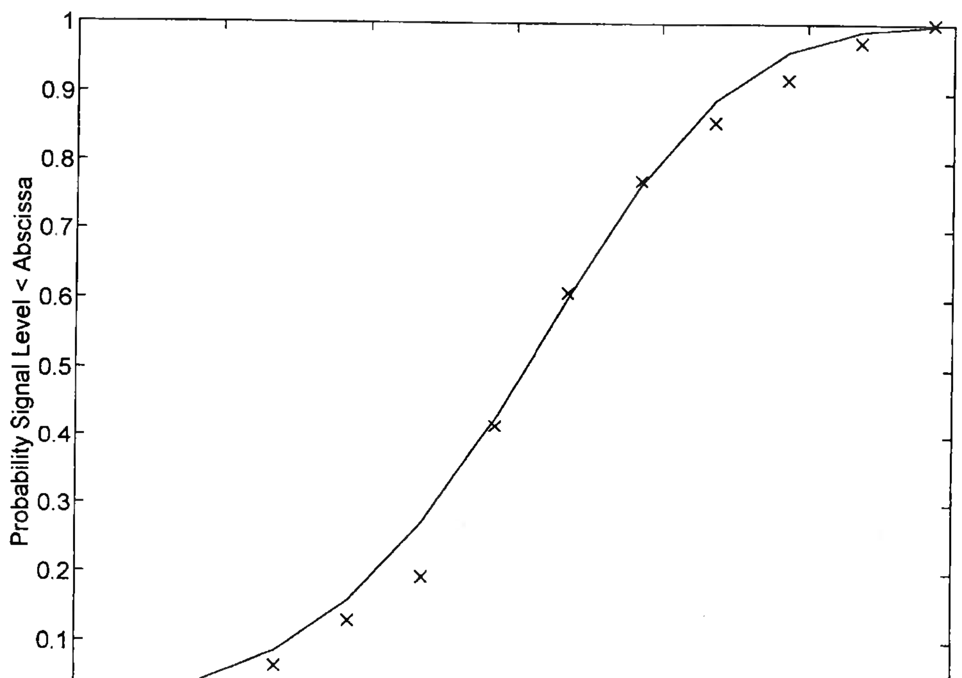


*Figure 29* - Comparison of the measured and theoretical cdf based on the Rice Factor k

### *3.2 Path Loss statistics*

For a fixed transmitter power ($P_t$) the received power ($P_r$) decreases with distance (d) as

$$P_r(d) = Ad^{-\alpha} \tag{1}$$

where $\alpha$ is the exponent of the power-distance relationship and A is a constant set by transmitted power and measurement system gain [12,13]. When logarithm of (1) is taken, the linear relation between $P_r$ [dB] and log(d) is

$$10\log_{10}[P_r(d)] = 10\log_{10}[A] - 10\alpha\log_{10}[d] \tag{14}$$

The power is averaged over all 500 points of the measured frequency response. Knowing this and the distance d, the resulting A and $\alpha$ can be found by line-fitting on the measurements with minimum square error in Excel (*Fig. 27*). In the previous section was explained how was extracted $\beta_0^2$, the power of the direct ray from the data. In Table II are given values for $\alpha$ for different environments and for the direct ray $\beta_0^2$. The r is the correlation between the measured and modeled, defined by:

$$r^2 = 1 - \frac{\sum_i \left(y_i - \hat{Y}_i\right)^2}{\left(\sum_i y_i^2\right) - \frac{\left(\sum_i y_i\right)^2}{n}} \tag{15}$$

where $y_i$ is a measurement sample, $Y_i$ is an approximation of that sample and n is the number of samples.

TABLE II
Values of $\alpha$, A[dB], derived from the linear regression of power [dB] on the 10 $\log_{10}$ of distance for each of the four global experiments and calculated from $\beta_0^2$

| Experi-ment | $\alpha$ | A[dB] | r | $\alpha(\beta_0^2)$ | A ($\beta_0^2$) | r |
|---|---|---|---|---|---|---|
| I1 | | | | | | |
| omni | 1.88 | -74.05 | 0.48 | 1.86 | -74.78 | 0.44 |
| dir | 1.87 | -59.65 | 0.88 | 1.87 | -59,64 | 0.89 |
| I2 | | | | | | |
| T up | 0.78 | -102.23 | 0.45 | 0.76 | -102.44 | 0.44 |
| T down | 1.27 | -81.92 | 0.72 | 1.27 | -81.93 | 0.72 |
| O1 | 1.9 | -72.21 | 0.99 | 1.91 | -72.2 | 0.99 |
| O2 | | | | | | |
| omni | 2.1 | -71.80 | 0.94 | 2.12 | -71.72 | 0.93 |
| dir | 2.54 | -48.03 | 0.8 | 2.55 | -17.99 | 0.79 |

*Fig 30.* shows the trendline for the environment O2 (parking). The $\alpha$ is almost 2, as for the free-space. Correlation *r* is 0.94.
From Table II it can be seen that the path loss factor is always around 2, but that not always a good correlation factor is found and thus those results are not so reliable. An explanation can be for the omni-directional corridor measurements (I1) that the *k* Factor is not so high and because of the multipath most of the signal remains in the corridor (waveguide-effect). Then the received power is not decreasing as fast as eq. (14), which makes (14) less valuable.
The amphitheater measurements (I2) were not in a straight line, but on random positions. That causes not only a decreasing power with distance as in eq. (14), but also different multipath fading from the same reflection objects (walls) and makes eq. (14) also less valuable.

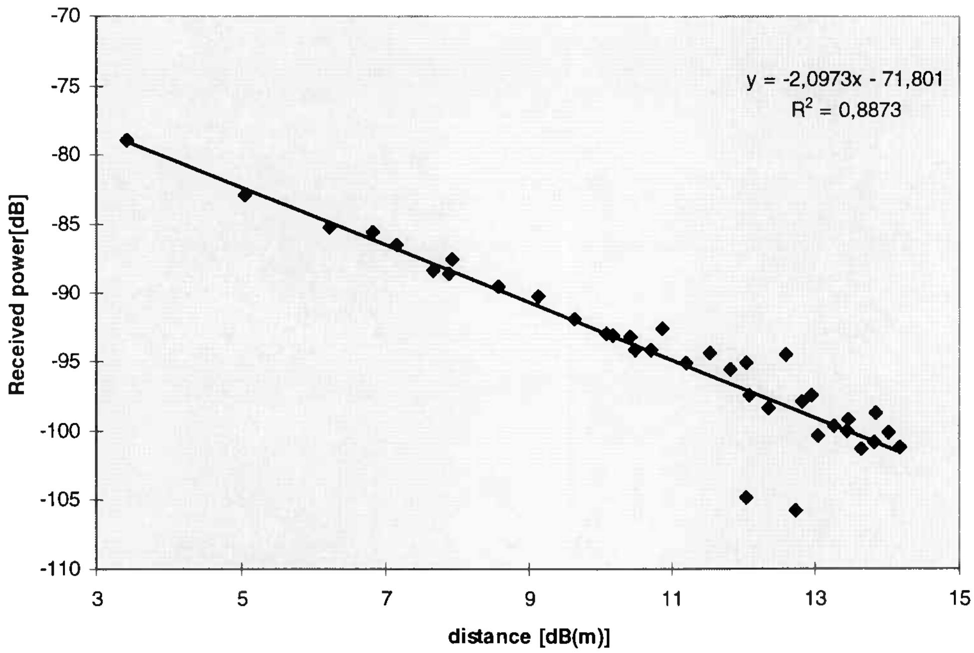


*Figure 30* - A scatter-plot of the measured power [dB] versus the distance on a log scale for experiment O2 (parking) with the omni-directional antenna. Also shown is the line with the minimum mean square error fit to the data.

### *3.3 Coherence bandwidth*

The coherence bandwidth is defined as that bandwidth over which the channel can be called constant/ flat, or not changing more than 3 dB. That is related to the correlation in the *frequency domain* of the different frequency components, which should be above 0.5.
The definition of the correlation is:

$$R(\Delta f) = \int_{-\infty}^{\infty} H(f) H^{*}(f + \Delta f) df \qquad (16)$$

Because we don't have the complete transfer function H(f) (only for a bandwidth of 100 MHz, and only the modulus or power/ amplitude version), an approximation is made by using a sliding window (first 250 samples of the measured bandwidth) over the same measured bandwidth. By correlating the measured 100 MHz bandwidth with this shifted window-version in Matlab (cor.m, appendix III) a correlation figure can be extracted, from which a figure for the coherence bandwidth can be extracted. The results showed however that for most of the spectra the correlation never came under 0.5. Simulations of a multipath fading channel showed the same results. That means that the coherence bandwidth is almost always bigger than 50 MHz (which is the maximum extractable coherence bandwidth, because of the window of 250 samples). When you look at the spectra of the measured bandwidths, there are drops of more than 3 dB, but they are not very broad. Eventually, only from the omni-directional measurements in the corridor which are most affected by multipath fading and thus are varying a lot, a few extracted coherence bandwidth's are below the 50 MHz. An example of a correlation figure for the amphitheater measurements is given in *Fig. 31.*

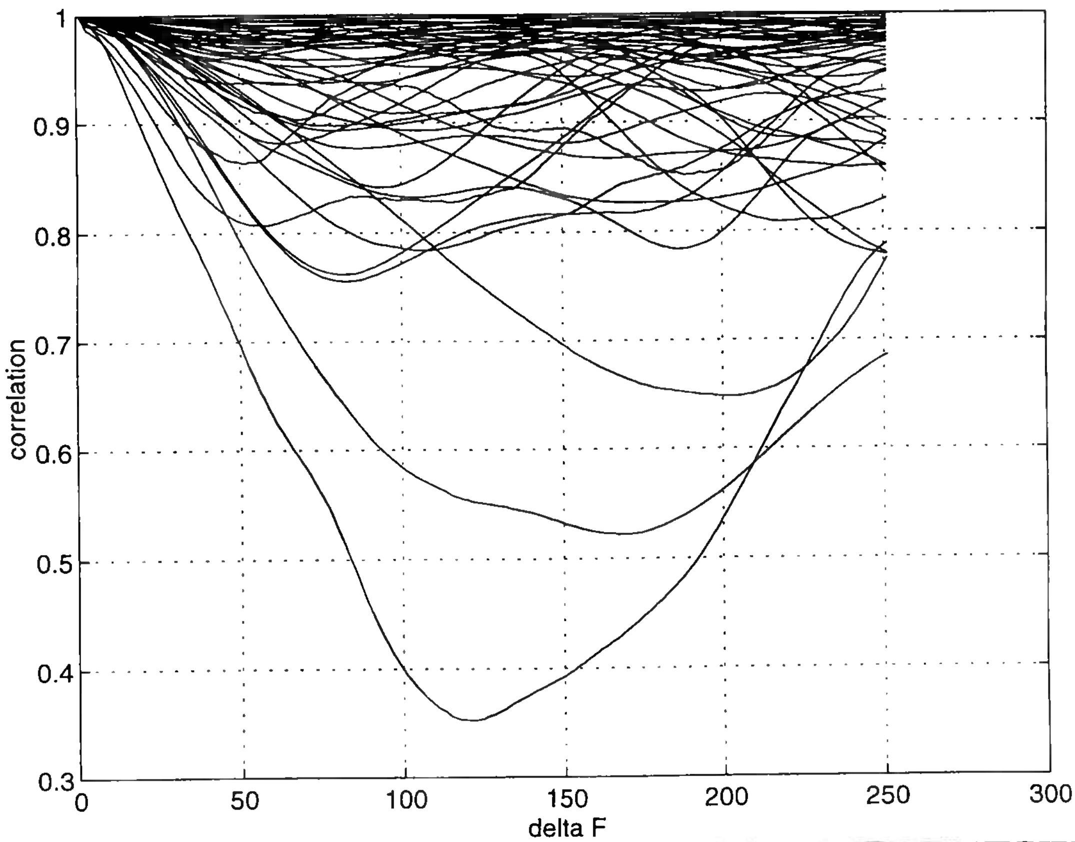


*Fig. 31* - Correlation figure of measurements from the amphitheater

### *3.4 Delay spread*

Because the coherence bandwidth calculations based on correlation in frequency domain didn't result into many details, another approach is made. A method to derive a figure for the delay spread is developed.

By analyzing the level crossing rate statistics of the measured spectra and fitting them to a theoretical model based on the root mean square (rms) delay spread and the Rice Factor $k$, the delay spread can be extracted. The processing of the level crossing statistics of the measured spectra was done in Matlab (lcr.m, appendix IV), just like the processing of the theoretical level crossing rate.

The theoretical level crossing rate is based on the following model (*Fig. 32*) of the delay power spectrum, [14]:

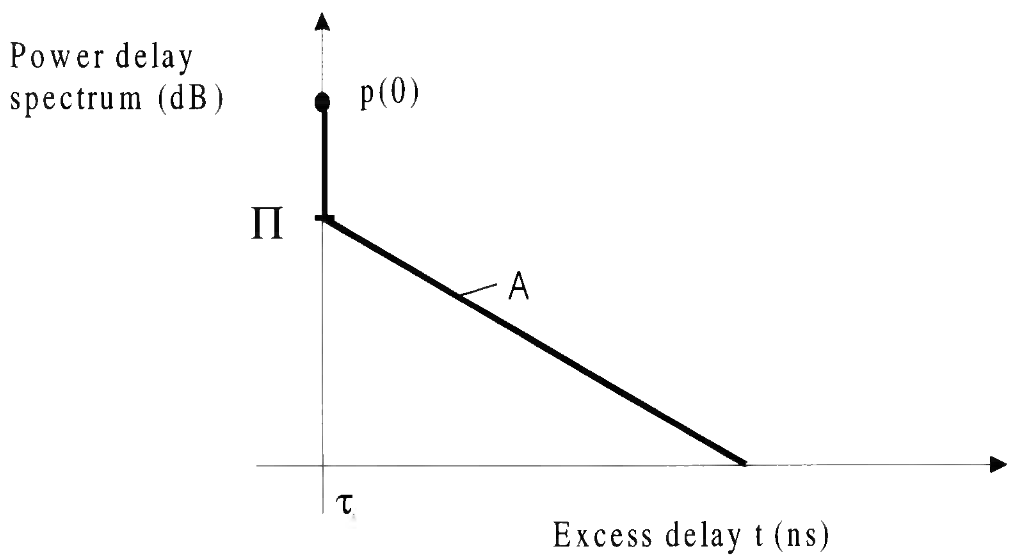


*Figure 32* - Model of the power delay spectrum (PDS)

The model is characterized by three parameters: *p(0)* [dB], the power of the direct ray, Π [dB/ns], the power-density of the constant-level part and A [dB/ns], the slope of the exponentially decaying part. $\tau_1$ [ns], the turning point is zero, in the case of our measurements $\tau_1$, because there was always a good alignment between the transmitter and receiver antenna. The three parameters are extractable from the normalized received power and Rice Factor $k$.
Because this model is based on a local area, only the wideband corridor measurements were tested on the model. Ten wideband samples from a local area (40 cm) were taken together as a set of measurement data to extract the level crossing statistics. These ten wideband spectra (which were corrected with a distance correction factor for the path loss differences) should be enough data to be accurate enough. With the Rice Factor $k$ and the normalized received power as input, the theoretical level crossing rate was compared with the level crossing rate pdf obtained from the measurements. The theoretical pdf was normalized to a rms delay spread of 1 ns. By viewing these 2 pdf's, a constant factor should be multiplied to the theoretical pdf to fit them. This multiplication constant is the actual rms delay spread that we're looking for. Examples of such plots are given in *Fig. 33*, for the omni-directional receiver antenna and *Fig. 34*, for the directional receiver antenna.

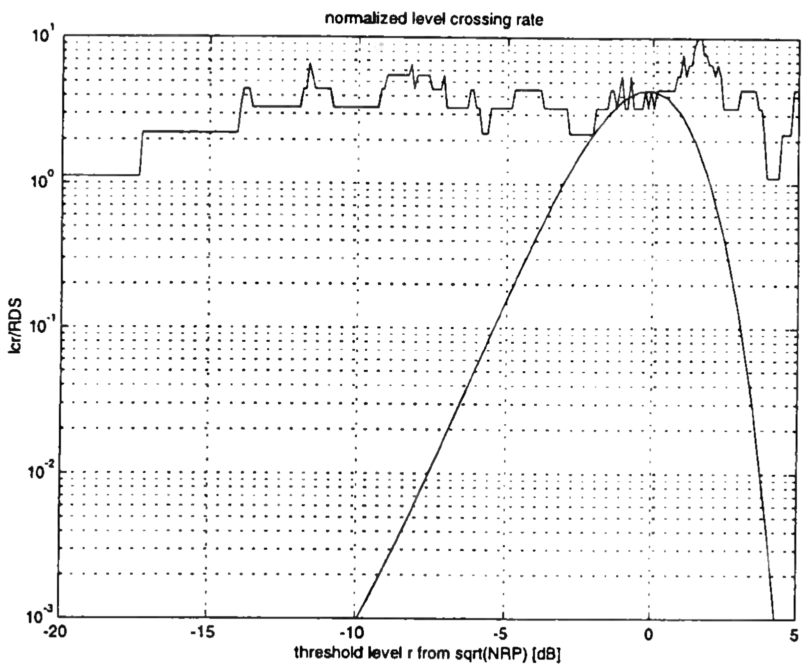


*Fig. 33* - Example of the fitting of the measured and theoretical (smoothed) pdf of the level crossing rate for the omni-directional receiver antenna measurements in the corridor

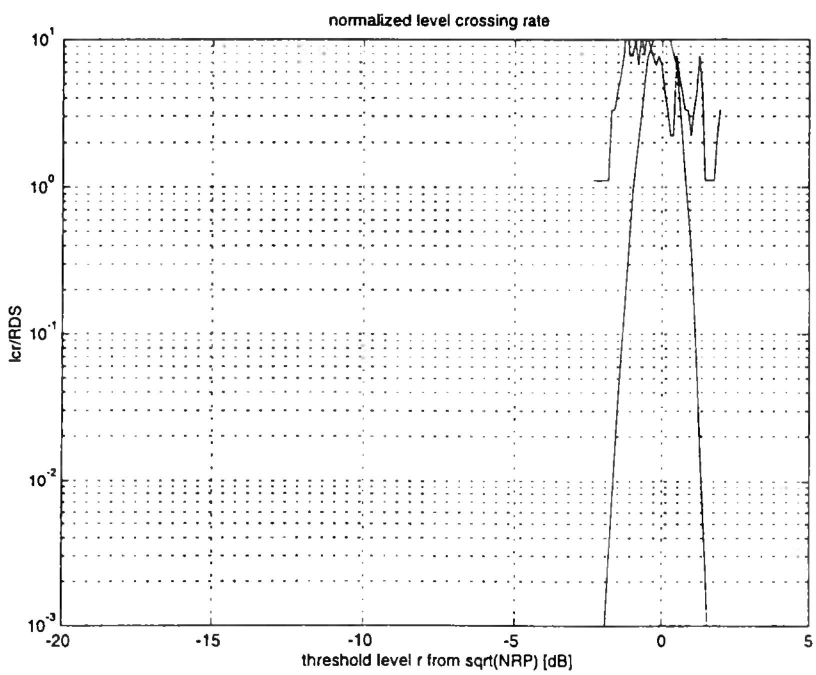


*Fig. 34* - Example of the fitting of the measured and theoretical (smoothed) pdf of the level crossing rate for the directional receiver antenna measurements in the corridor

These plots show that the fit isn't that nice as was expected. Especially the lcr results from the omni-directional antenna measurements are much broader than the theoretical lcr. The directional measurements are a little bit better, but not quite fitting well either. The only conclusion that can be drawn from these measurements is that the delay spread is in the order of nano-seconds. This is also an explanation why the coherence bandwidth-extraction didn't yield useful results. The coherence bandwidth is proportional to the inverse of the rms delay spread and should therefore be in the order of hundreds of MHz.

Obviously, the assumption that the set of 40 cm is a local area is not valid. In the future, measurements within a real local area (within wavelengths, that is: < 10 cm) should be processed to see if these measurements are suitable for fitting on the theoretical level crossing rate.

For a comparison, a lcr fitting of local measurements (within the 10 cm) is given in *Fig. 35*. In this figure it can be seen that the fitting is much more smoothly.

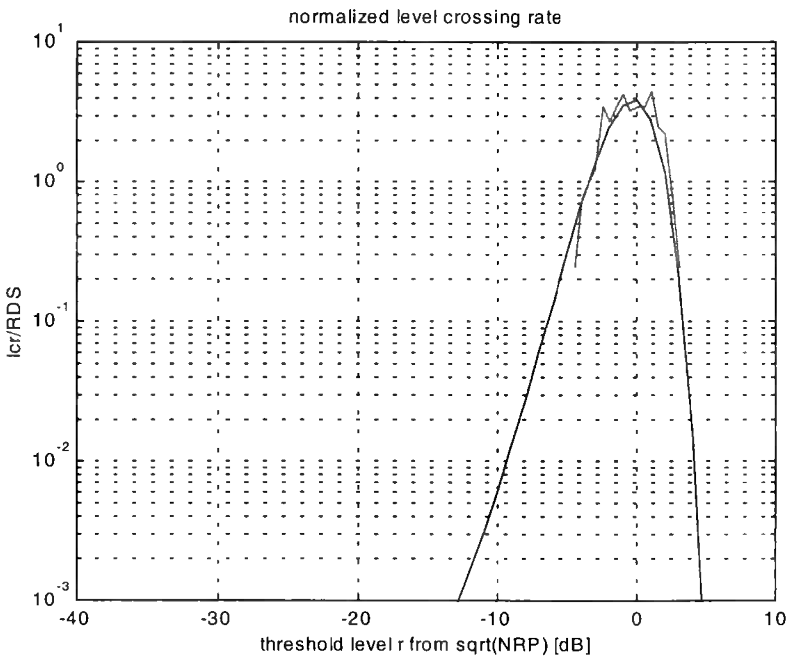


*Fig. 35* - Example of the fitting of the measured and theoretical (smoothed) pdf of the level crossing rate for local measurements

# 4. Conclusions & Recommendations

## *4.1 Conclusions*

In order to get a better understanding of 60 GHz propagation effects in different environments with different conditions, Carrier Wave and Wideband (100 MHz bandwidth) frequency measurements using a spectrum analyzer were performed. These experiments were performed in a corridor and room on the 19th floor, a big college room in a 22-floor office building of the Department of Electrical Engineering, Delft, The Netherlands (indoor) and at a parking and a grassfield at the side of that building (outdoor), as being possible locations for the mobile multimedia communication. Both an omni-directional and a directional receiver antenna were used to experience the difference.
With these measurement data, methods to derive the following parameters are developed:

- path-loss characteristic
- Rice factor *k*
- coherence bandwidth
- level crossing rate statistics
- order of RMS delay spread

An overview of the measurements and extracted results is given in Table III.

TABLE III
List of all measurements at different environments and obtained results

| Type | Place | Type R antenna | Positions | Results |
|---|---|---|---|---|
| Moving CW | Corridor<br>Room | Omni-dir. | 0m80 .. 24 m<br>4 different circles | Power spectrum |
| CW | Corridor | Omni-dir. | every 0,5 m 9 x 2,5 mm from 0m50 .. 17m<br>6m00 .. 7m00 (every mm) | Path Loss<br>Power spectrum |
| Wideband | Corridor | Omni-dir. | 5m00 .. 11m00 ( every 4 cm)<br>11m00 .. 43m00 (every m) | Path Loss<br>Rice Factor *k*<br>Delay spread |
| | | Dir. | 5m00 .. 11m00 ( every 4 cm)<br>11m44 .. 43m44 (every m) | Path Loss<br>Rice Factor *k*<br>Delay spread |
| | Amphitheater | Omni-dir. | T antenna up, 50 positions<br>T antenna down, 50 positions | Path Loss<br>Rice Factor *k* |
| | Outdoor (grassfield) | Omni-dir. | 1m00 .. 27m00 (every m) | Path Loss<br>Rice Factor *k* |
| | Outdoor (parking) | Omni-dir. | 2m20 .. 26m20 (every m)<br>12 spread positions | Path Loss<br>Rice Factor *k* |
| | | Dir. | 3m20 .. 24m20 (every m)<br>15 spread positions | Path Loss<br>Rice Factor *k* |

The following conclusions can be drawn from the previous chapters:

- The environment plays an important role in the radio propagation of a 60 GHz channel; the more reflection walls/ obstacles in close neighborhood of the wireless channel, the more hostile will the communication channel be
- Omni-directional antennas are far more sensitive to multipath fading than directional antennas and cause more "drops" in the received frequency spectrum
- Mobility causes the received power to fluctuate
- It doesn't appear that weather conditions like temperature and wind play a role in the propagation of radio-waves at 60 GHz
- Radio coverage up to 40 meter is achievable, probably even more
- The path loss exponent was always around 2 (as for free space propagation)
- The Rice factor $k$ varies from around 15..60 for an omni-directional receiver antenna to 200..400 for a receiver directional antenna
- The coherence bandwidth of almost all measurements exceeded the 50 MHz, therefore OFDM with it's multiple (small band) carriers is very suitable for 60 GHz communication
- The delay spread was in the order of nanoseconds
- With the extracted parameters as path loss, Rice factor $k$, coherence bandwidth and delay spread a global description of the channel is possible

### *4.2 Recommendations*

Because the measurements were too much separated in distance and not in a local area, the extracted results are just a global description of the channel. They just give a figure of what you can expect. That's why for further analysis of the 60 GHz communication channel more and denser (more in the order of some wavelengths) measurements are needed. With this information a better understanding of especially multipath fading, which is a major aspect of the wireless communication channel, can be obtained.

By making more and more dense measurements the validity of the in this report used methods to extract channel parameters and thus the parameters itself can be checked and if needed adjusted.

Especially, the level crossing rate method that extracts the rms delay spread is not really tested on its validity and could yield more detailed information about the delay spread. If the results are satisfying, the model of the power delay spectrum as described in the paragraph "Delay spread" of the chapter "Measurement analysis" can be used to model the wireless communication channel.

For the coherence bandwidth extraction method, measurements with more bandwidth (in the order of a GHz) should be made, although that requires expensive equipment.

To see if the fact that no information is available about the phases of the propagation rays is too much of an approximation, other measurement methods which include this information and other modeling methods like Ray tracing [15] could be performed for comparison.

Each environment has a different impact on the radio propagation. Therefore a classification of environment models can be used (for example: indoor small (room), indoor big (hall), outdoor (open), outdoor (obstructed)). By measuring several environments for every classification you must be able to see if it fits in the classification and if needed extend the classification. Within each classification many (and dense) measurements contribute to an accurate type of modeling. Always try to think of a practical classification of these environments, in other words: think of environments in which the wireless communication system at 60 GHz actually is going to be used.

The measurements done in the corridor were done nearly in the middle of the corridor. Strange effects can occur in the middle (although they were not mentioned in our measurements), because different traveling paths can have exactly the same distance (through the walls at both sides of the corridor). Therefore it is better to measure away from the middle. Then a more typical corridor measurement can be performed.

Measurements were done quite automatic, but the moving of the antenna was done manually. By using the rail, measurements become more accurate and easier and faster to carry out. Another improvement towards automation of the measurements could be obtained by synchronizing the signal generator to the rest of the measurement system. Every step towards more automation of the measurements yields more time-savings and accuracy.

# Appendix I : Extracting Rician Factor *k* out of measured power spectrum |H(f)|$^2$

How can we extract the Rician Factor *k* out of a measurement data file with the Received power over a spectrum of 100 MHz ?
Therefore we use the mean and variation of the received power of the measured power spectrum as input for two equations with two unknown variables; namely, the wanted Rician Factor *k* and the amplitude of the Line-Of-Sight component $\beta_0$.

The first equation we get from the definition of the Rician Factor *k* as the ratio of the powers of the Line-Of-Sight component (direct ray) and the interfering components (all reflected rays);

$$k \stackrel{\Delta}{=} \frac{\beta_0^2}{\sum_{m=1}^{N} \beta_m^2} \tag{9}$$

where $\beta_0$ is the direct path amplitude and $\beta_m$ is the amplitude gain of each propagation component. The definition of the mean of the received power is the mean of the squared amplitude transfer function;

$$\overline{|H(f)|^2} = \overline{P} = \sum_{m=0}^{N} \beta_k^2 \tag{8}$$

If we combine these two definitions, we get the first formula of the two that we need;

$$\overline{P} = \left(\frac{k+1}{k}\right)\beta_0^2 \tag{10}$$

The second formula we can derive from the variation of the received power;

$$\sigma_{P(f)}^2 = \overline{P^2(f)} - \left(\overline{P(f)}\right)^2 \tag{11}$$

where $\sigma_{P(f)}^2$ is the variance of *P(f)*, which can also be extracted from the wideband measurements. Using (8), we get

$$\left(\overline{P(f)}\right)^2 = \left(\sum_{i=0}^{N} \beta_i^2\right)^2 = \sum_{0}^{N} \beta_i^4 + \sum_{i \neq j,0}^{N} \sum_{j=o}^{N} \beta_i^2 \beta_j^2 \tag{17}$$

and

$$\begin{aligned} P^2(f) = |H(f)|^4 &= \left(\sum_{i=0}^{N} \sum_{j=0}^{N} \beta_i \beta_j e^{j((2\pi f(\tau_i - \tau_j)) + (\theta_i - \theta_j))}\right)^2 \\ &= \left(\sum_{i=0}^{N} \beta_i^2 + \sum_{i \neq j,0}^{N} \sum_{j=0}^{N} \beta_i \beta_j \cos\alpha_{ij}\right)^2, \alpha_{ij} = 2\pi f(\tau_i - \tau_j) + (\theta_i - \theta_j), \alpha_{ij} = -\alpha_{ji} \end{aligned} \tag{18}$$

The average is then:

$$\overline{P^2(f)}=\overline{\left(\sum_{i=0}^{N}\beta_i^2\right)^2}+\overline{2\sum_{i=0}^{N}\sum_{j=0}^{N}\sum_{k=0}^{N}\beta_i^2\beta_j\beta_k\cos\alpha_{jk}}+\overline{\left(\sum_{i\neq j,0}^{N}\sum_{j=0}^{N}\beta_i\beta_j\cos\alpha_{ij}\right)^2} \tag{19}$$

The second term is zero, because of the cos-term. The other two terms yield:

$$\overline{\left(\sum_{i=0}^{N}\beta_i^2\right)^2}=\sum_{i=0}^{N}\beta_i^4+\sum_{i\neq j,0}^{N}\sum_{j=o}^{N}\beta_i^2\beta_j^2 \tag{20}$$

$$\overline{\left(\sum_{i\neq j,0}^{N}\sum_{j=0}^{N}\beta_i\beta_j\cos\alpha_{ij}\right)^2}=\overline{2\sum_{i\neq j,0}^{N}\sum_{j=0}^{N}\beta_i^2\beta_j^2\cos^2\alpha_{ij}}+\overline{\sum_i\sum_j\ldots\cos\alpha_{ij}}=2*1/2*\overline{\sum_{i\neq j,0}^{N}\sum_{j=0}^{N}\beta_i^2\beta_j^2} \tag{21}$$

Substituting (20) and (21) in (19) yields:

$$\overline{P^2(f)}=\sum_{i=0}^{N}\beta_i^4+2\overline{\sum_{i\neq j,0}^{N}\sum_{j=0}^{N}\beta_i^2\beta_j^2} \tag{22}$$

Substituting (22) and (17) in (11) yields:

$$\sigma_p^2=\sum_{i\neq j,0}^{N}\sum_{j=0}^{N}\beta_i^2\beta_j^2=\left(\sum_{i=0}^{N}\beta_i^4+\sum_{i\neq j,0}^{N}\sum_{j=0}^{N}\beta_i^2\beta_j^2\right)-\sum_{i=0}^{N}\beta_i^4=\left(\sum_{i=0}^{N}\beta_i^2\right)^2-\sum_{i=0}^{N}\beta_i^4 \tag{23}$$

and the first term is:

$$\left(\sum_{i=0}^{N}\beta_i^2\right)^2=\left(\beta_0^2+\sum_{i=1}^{N}\beta_i^2\right)^2=\left(\beta_0^2+\beta_0^2/k\right)^2=\left(\beta_0^2(1+1/k)\right)^2 \tag{24}$$

When k > 6, the following approximation can be made:

$$\sum_{m=0}^{N}\beta_m^4\cong\beta_0^4 \tag{12}$$

Substituting (12) and (24) in (23) yields the second equation we were looking for:

$$\sigma_{P(f)}^2=\frac{2k+1}{k^2}\beta_0^4 \tag{13}$$

If we combine the two equations (10) and (13) with the two unknown variables, we can extract the Rician Factor *k* out of the resulting equation:

$$\sigma_p^2k^2+\left(2\sigma_p^2-2\overline{P(f)}\right)*k+\left(\sigma_p^2-\overline{P(f)}\right)=0 \tag{25}$$

There are two roots of the equation but one is always in the neighbourhood of zero and that's not what we expect in practice (where a LOS always existed). The other has to be the right one then.

With the known Rice Factor *k* we can calculate the Line-Of-Sight component $\beta_0$ with eq. (10) or (13). The processing of the extracting method is done in Matlab (extractk.m, see Appendix II).

# Appendix II: Extractk.m (Matlab program) - Rice Factor *k* extraction

```
% Matlab Program name: Extractk.m
%
% Goal: To extract the Rice factor K (mean and variation)
%       out of the wideband measurements
%
% Input: Data-files of wideband measurements named as .......1 (e.g. point1)
%                                                      .......2
%                                                      etc.
%
% Output: Rice factor K (mean and variation) for an environment
%
% Date:  jan. '98
%
% Author: Arthur Mank


% Initialization
Rice= [];
Energy = [];
k = 0;
Gem = [];
Disc = [];
Vari = [];
% Type the filename in: for example, point, if files are called point1, point2 etc.
name=input('What is the name of the file (without number) ? ', 's')

while 1                    % always, unless file doesn't exist

% Take file k (k=1, 2 .... )
k = k+1;
datak = [name int2str(k)]
filename = [datak '.dat']
if ~exist(filename), break, end

% If file exist: Read info, then data
fid=fopen(filename ,'r');
ExperDate=fscanf(fid,'%s',1);
ExperTime=fscanf(fid,'%s',1);
ExperData=fscanf(fid,'%s',1);
ExperCenterFreq=fscanf(fid,'%s',1);
ExperBandwidth=fscanf(fid,'%s',1);
dummy=fscanf(fid,'%s',1);
data=fscanf(fid,'%g',inf);

% Close file
status=fclose(fid);
```

```
% From dBm (exponential) to W (linear)
datal=0.001*10.^(data/10);

% Process data (Extract mean and variance)
gem = mean (datal);
var = (std (datal))^2;

% Put mean and variance in a matrix
gem2 = 10*log10(1000*gem);
Gem = [ Gem gem2 ];
Vari = [ Vari var ];

% Calculate K and B0
K = roots ( [var (2*var-2*gem^2) (var-gem^2)] );  % yields 2 k-values
B0 =  K.*gem ./ (K+1) ;                             % yields 2 B0^2-values

% Add K-value to Rice-matrix and B0's to Energy-matrix
Rice = [ Rice K ]
Energy = [ Energy B0 ]
end

% Take mean and variance of K-values
Kgem = mean (Rice')
Kvar = (std (Rice'))^2

% Make a plot of the k-values
plot(Rice')
ylabel('Rician Factor K')
```

# Appendix III : Cor.m (Matlab program) - Correlation figure extraction

```
% Matlab Program name: cor.m
% This program makes a correlation figure of the measured wideband data
% in order to determine coherence bandwidth
% INPUT VALUES: field strength for 500 different frequencies in [dBm] spread over 100
% MHz bandwidth from file [wideband sample].DAT (tab delimited file)
% OUTPUT VALUES: correlation figure, a MATLAB graph.
% DATE: 21 March '98
% AUTHOR: Arthur Mank, TVS group, TU Delft


clear;
clf;

fid=fopen('Hchan.dat','r');          % opens data file for reading
DATA=fscanf(fid,'%g',inf);
status=fclose(fid);                  % closes data file

DATA=0.001*(10.^(DATA/10));          % from dBm to W
DATA=sqrt(DATA);                     % from W to V

% doing the correlation

N=length(DATA);                      % 500 length of the sequence to be corellated
Window=250;
Norm=DATA(1:Window)'*DATA(1:Window); % define the normalization constant
for deltaF = 0:N-Window;             % deltaF=1:250
  SUM=0;                             % calculate the correlation at deltaF
  for i=1:Window;
      SUM=SUM+DATA(i)*DATA(i+deltaF);
  end;
  CORR(deltaF+1)=SUM;                % Add to the correlation vector
end;

CORR=CORR/Norm;                            % Normalize the correlation vector

figure(1);
plot (CORR);
hold on;

xlabel ('delta F');
ylabel ('correlation');
title ('correlation, 60 GHz, 100 MHz BW');
```

# Appendix IV : Lcr.m (Matlab program) - Level crossing rate pdf extraction

```
% Matlab Program name: lcr.m
%
% Goal: To extract the level crossing rate characteristics
%       out of the wideband measurements
%
% Input: Data-files of wideband measurements named as .......1 (e.g. point1)
%                                                       .......2
%                                                       etc.
%
% Output: "Pdf" of level crossing rate for an environment
%
% Date:  May '98
%
% Author: Arthur Mank


% Initialization
        n=10;                   % File is "n"m"k"
        k=60;
        m=0;
        if k==0
                p=n+1;
        else
                p=n;
        end;
        r0= p + k/100;          % Normalised distance
        minu = -79;             % Minimum Level
        maxu = -58;             % Maximum Level
        step = 0.1;
        size = (maxu-minu)/step;
        Lcrn = zeros(1,size+1);
% Type filename: m
        name=input('What is the name of the file (without number) ? ', 's')

  while 1                       % always, unless file doesn't exist

% Take file k (k=1, 2 .... 10 ) 10 measurement spectra
        m=m+1;
        if k==00,
                n = n+1;
                datak = [int2str(n) name int2str(k) int2str(k)];
                else
                datak = [int2str(n) name int2str(k)];
        end
        filename = [datak '.dat']
```

```
        if (~exist(filename) | m==11), break, end
        correction=((n+k/100)/r0)^2                % Correction with normalized distance
        if k<96,  k= k+4;,   else k=00;, end

% If file exist: Read info, then data
        fid=fopen(filename ,'r');
        ExperDate=fscanf(fid,'%s',1);
        ExperTime=fscanf(fid,'%s',1);
        ExperData=fscanf(fid,'%s',1);
        ExperCenterFreq=fscanf(fid,'%s',1);
        ExperBandwidth=fscanf(fid,'%s',1);
        dummy=fscanf(fid,'%s',1);
        data1=fscanf(fid,'%g',inf);

% Close file
        status=fclose(fid);

% From dBm (exponential) to W (linear), distance corrected and back to exponential (dBm)
        data2=0.001*10.^(data1/10);
        data3=correction*data2;
        data4=log10(data3*1000)*10;
        data = data4;
        figure(1);
        plot(data1);                % Plot original measurement data
        hold on;

        figure(2);
        plot(data4);                % Plot distance corrected data
        hold on;

% "Smoothing" / Noise filtering with 50-sample-averaging window
        for i = 1 : 451
                datal(i) =
(data(i+49)+data(i+48)+data(i+47)+data(i+46)+data(i+45)+data(i+44)+data(i+43)+data(i+42)
+data(i+41)+data(i+40)+data(i+39)+data(i+38)+data(i+37)+data(i+36)+data(i+35)+data(i+34)
+data(i+33)+data(i+32)+data(i+31)+data(i+30)+data(i+29)+data(i+28)+data(i+27)+data(i+26)
+data(i+25)+data(i+24)+data(i+23)+data(i+22)+data(i+21)+data(i+20)+data(i+19)+data(i+18)
+data(i+17)+data(i+16)+data(i+15)+data(i+14)+data(i+13)+data(i+12)+data(i+11)+data(i+10)
+data(i+9)+data(i+8)+data(i+7)+data(i+6)+data(i+5)+data(i+4)+data(i+3)+data(i+2)+data(i+1
)+data(i))/ 50;
        end;
        figure(3);
        plot(datal(1:451));         % Plot smoothed spectrum
        hold on;


% Determine level crossing rate
        Lcr = [];
        step = 0.1;
```

```
        for i = 0 : size
                level = minu + i*step;
                nr = 0;
                for i = 2 : 451
                        sign1 = (datal(i) < level);
                        sign2 = (datal(i-1) > level);
                        if (sign1==1 & sign2==1)
                                nr=nr+1;
                        end;
                end;
                Lcr = [Lcr nr];
        end;
        Lcrn = Lcrn + Lcr;              % add to lcr-vector
end;

Lcro = Lcrn / (m-1);                    % Normalize with nr. of spectra
hold off;

% save lcr = # times sign. level crosses lcr level
save Lcr1.dat Lcro -ascii

% Plot lcr against the level (pdf)
        Level1= minu:step:maxu;
        figure(4);
        plot (Level1, Lcro);
        ylabel ('Level Crossing Rate');
        xlabel ('amplitude level');
        title  ('pdf of Level Crossing Rate (not normalized)');
```

Extension :

```
% Program name : lcr2.m
%
% Goal : Extension of lcr.m : To adjust lcr-vector from lcr.m in the same format
%                              as the theoretical lcr-vector
%
% Input : Data-files of wideband measurements named as  .......1 (e.g. point1)
%                                                        .......2
%                                                        etc.
%
% Output : "Pdf" of level crossing rate for an environment
%
% Date :  May '98
%
% Author : Arthur Mank


% Initialization
        minu = -80;             % Minimum Level
```

```
        maxu = -50;             % Maximum Level
        nrp = -55.803;          % Normalised received power
        minu = minu - nrp;      % Normalise with nrp
        maxu = maxu - nrp;
        step = 0.1;
        size = (maxu-minu)/step;
        Level= minu:step:maxu;

% Open Lcr-vector
        load lcr1.dat;

% Normalize to 1 GHz
        lcr1=lcr1*100/9;

% Plot against received power Level
        semilogy(Level, lcr1);
        xlabel('Power Level (dB)');
        ylabel('Level Crossing Rate (dB/GHz)');
        title('pdf of Level Crossing Rate');
        hold on;
```

## References

[1] R. Prasad and L.M. Correia, “An overview of Wireless Broadband Communications”, *IEEE Communications Magazine*, Jan. 1997

[2] R. Prasad and L. Vandendorpe, *An overview of Millimeter Wave Indoor Wireless Communications Systems*, Fac. Electrical Engineering, TU Delft, 1996

[3] W.C. Lee, “Mobile communication design fundamentals”, 2. Ed, John Willey & Sons, 1993, ISBN 0-471-57446-5

[4] T.S. Rappaport, "Wireless communications; principles and practice", Prentice-Hall, 1996, ISBN 0-13-375536-3

[5] B. Sklar, “Rayleigh fading channels in mobile digital communication systems, part I: Characterization, part II: Mitigation”, IEEE Communications Magazine, pp. 90-109, July 1997

[6] A. Polydrou and G. Stratakos, “Comparative study of millimeter wave propagation at 30 GHz and 60 GHz in indoor environment”, *International Journal of Infrared and Millimeter Waves,* Vol. 16, No. 10, 1995

[7] P.M.F. Smulders, “Broadband wireless LANs: A feasibility study”, Ph.D. thesis, Eindhoven university of Technology, The Netherlands, ISBN 90-386-0100-X, 1995

[8] P.E. Leuthold and P. Truffer, “Indoor radiowave propagation measurements and stochastic channel modeling” *Proc. of the IRCTR colloquium on indoor communications*, Delft, The Netherlands, 1997

[9] D. Matic, H. Harada, H. Reijmers, “Measurements of the indoor spatial distribution of the radio-field level for mm-waves in the range of 60 GHz”, *Proc. IEEE VTC' 98,* pp. 82-88, Oct. 13-15, 1997, Enschede, The Netherlands, ISBN 90-365-10570

[10] F. van der Wijk and A. Kegel, “Assessment of a pico-cellular system using propagation measurements at 1.9 GHz for indoor wireless communications”, *IEEE Transactions on vehicular technology”*, vol.44, No.1, Feb. 1995

[11] P. Vasconcelos and L.M. Correia, “Fading characterization of the mobile radio channel at the millimetre waveband”, *Proceedings. of the VTC '97*, pp. 999-1003, Phoenix, Arizona, USA, May 1997

[12] S.J. Howard and K. Pahlavan, “Measurement and analysis of the indoor radio channel in the frequency domain”, *IEEE Trans. Instrumentation and measurement,* vol. 39,pp. 751-755, Oct. 1990

[13] L. Correia and J. Reis, “Analysis of the average power to distance decay rate at the 60 GHz band”, *Proceedings of the VTC'97,* p.994-998, 1997

[14] K. Witrisal, Y. Kim and R. Prasad, “Frequency domain simulation and analysis of the frequency-selective Ricean fading radio channel”, *Proceedings PIMRC' 98,* Boston 1998

[15] K. Tzimeas, “A deterministic indoor propagation prediction technique using ray tracing and field measurements at 60 GHz”, Thesis report, TU Delft, 1997